

Rohingya refugee camps and land cover change in Bangladesh*

Colette Salemi[†]

November 11, 2025

Abstract

How does the rapid establishment of a large-scale refugee camp affect competition for land and, consequently, local land cover? I examine this question in Bangladesh using high-resolution Dynamic World data (2016-2023) on Cox Bazar, a district hosting the largest refugee camp in the world. The analysis focuses on areas within 0–5 km of camp boundaries, using propensity score matching to define counterfactuals and a difference-in-differences event study framework to estimate impacts. The 2017 Rohingya refugee influx and related camp expansions reduced forest cover by 4.6 percentage points by 2019, but forests partially recovered in subsequent years. Settlement cover grew steadily, reaching 3.7 points in 2022. Results are robust across multiple specifications. Heterogeneity analysis shows that effects are strongest near the Kutupalong expansion site. Early forest losses were likely driven by biofuel extraction, while recoveries may reflect LPG cookstove programs, fencing, or both. Increases in nighttime lights indicate that settlement expansion reflects local economic growth following camp establishment.

Keywords – Refugee camp; land cover impacts; general equilibrium effects; Rohingya refugees; Bangladesh; Cox Bazaar

*The author would also like to thank Stephen Polasky, Daniel Rondeau, Marc F. Bellemare, Khandker Wahedur Rahman, and Justin Johnson for feedback on the draft. The author thanks Nfamara Dampha: a 2020-2022 collaboration with him introduced the author to this topic, and this study is an extension of that effort, which is available as World Bank Policy Research Working Paper #9948. An additional thanks to participants at seminars hosted by the University of Minnesota's department of Applied Economics, Syracuse University's Maxwell School of Citizenship and Public Affairs, and the Ostrom Workshop at Indiana University. The author also thanks participants at the Canadian Economic Association and Canadian Agricultural Economics Association annual meetings, as well as the Australasian Development Economics conference, for their feedback.

[†]University of Victoria. Email: csalemi@uvic.ca.

1 Introduction

In late 2017, the Cox Bazar district of Bangladesh experienced a rapid influx of refugees. Rohingya peoples of Myanmar, driven from their villages by targeted military and extremist violence, crossed the border into Bangladesh in pursuit of asylum. In just a few months, over 700,000 Rohingya made this crossing, and new refugee camp areas rapidly emerged in the district. Today, these camps are among the largest and most overcrowded in the world, with the largest encampment area hosting a population density exceeding that of Dhaka, one of the most densely populated cities on the planet.

Since the first months of the 2017 arrival, media outlets, UN agencies, and the Government of Bangladesh have expressed concerns over the environmental impacts of this population influx. In heavily deforested Bangladesh, the districts of the Chittagong division (where Cox Bazar is located) are home to much of the country's remaining in-tact forests. Weeks after the influx began, local media outlets expressed concerns about the role of biofuel harvesting in driving forest losses in the camp areas. For example, an October 2017 article from Radio Free Asia reported that refugees had already cut down over one million trees for energy and shelter materials ([BenarNews, 2017](#)). These claims echo broader conjecture about the environmental impacts of refugee camps. For example, the United Nations High Commissioner for Refugees (UNHCR) claims that 20-25 million trees are cut down in and near refugee camps globally each year and that 90% of this harvest is used for fuelwood consumption ([UNHCR, 2022](#)). These figures are not supported by publicly available evidence.

The objective of this study is to use high-resolution geospatial data in combination with causal inference methods to estimate the local land use/land cover (LULC) impacts of refugee encampment. Using 10-meter Dynamic World LULC data, in combination with a matching difference-in-differences event study methodology, I examine the impact of the late 2017 Rohingya population influx on land cover characteristics. I use the area 0-5 km outside of camp boundaries as the treatment area because this is where agglomeration effects [d'Errico et al. \(2022\)](#); [Taylor et al. \(2016\)](#) and refugee biofuel harvesting are most

likely to manifest. To avoid contamination of the control group, I omit areas > 5 km and ≤ 20 km from a camp boundary.

I examine heterogeneity by protected area status, and I also estimate the results restricting the treated area to the 0-5km area in the vicinity of the Kutapalong Expansion Site, which hosts the largest refugee population. To evaluate the robustness of my findings, I repeat my estimation procedure using an alternative treatment group definition (0-10 km), using an adjacent district as my comparison area for matching, and omitting a politically dissimilar subdistrict from my sample. I explore mediating factors using secondary information on contemporaneous interventions, as well as an analysis of how the camps influence nighttime light radiance.

My inclusion of a robust identification strategy distinguishes this work from most of the recent efforts to examine Rohingya refugee-associated forest losses in Cox Bazar. Past research largely uses geospatial data and simple before-after comparisons to examine changes, directly assuming that any change in characteristics must be directly due to refugee activity (Hasan et al., 2021; Rahman et al., 2018; Sarkar et al., 2023). My study is an offshoot of Dampha et al. (2022), which used four years of Landsat data to predict a broad LULC classification for the district and applied discrete cutoffs to define both treatment and control areas as part of a DID estimation strategy. I improve upon this work by using a spatial data source with less measurement error for the region¹. I also use matching methods to improve on the robustness of the counterfactual sample and its trends.

Following Dampha et al. (2022), Roza et al. (2024) conducted an analysis that includes a brief evaluation of forest cover and nighttime lights in relation to proximity to refugee camps. My study extends this line of research through its specific focus on the local area immediately adjacent to the camps, rather than the broader regional trends. In addition, I use a higher resolution LULC product, which helps mitigate known sources of measurement error in lower resolution global products such as Hansen's Global Forest

¹Further assessment demonstrated considerable measurement error in the data used by Dampha et al. (2022), with settlement cover particularly over-estimated, including in regions in which cross-checking revealed no shelters. Another issue is that these LULC maps do not distinguish between forest and non-forest vegetation: the clearing of these different vegetation types have different implications. Please contact the author if you would like to see comparison maps that further demonstrate the higher representativeness of the Dynamic World data. The results of this cross-checking are not included in the present study.

Watch, including the misclassification of deforestation events ([Alix-Garcia and Millimet, 2023](#)). I also rely on masked annual VIIRS nighttime lights rather than the harmonized DMSV-VIIRS product, in order to capture finer-grained variation in low-radiance settings. This is particularly important in this context, where average radiance in the district overall in 2017 was just 0.21, and rounding in the harmonized product could obscure meaningful differences².

In the local area 0-5 km outside of camps, I find that following the August 2017 population influx and resulting camp creation, forest cover declines by 4.6 percentage points (p.p.) by 2019. Forest cover then shows signs of marginal recovery that may be related to a 2019 refugee-targeting LPG cookstove rollout or the 2019-2020 enclosure of the camps in fencing. The same pattern of loss and recovery is discernible in protected areas, though the magnitude of the effect is smaller. From 2018 to 2023, settlement cover continually expands throughout the region, with a measured increase of 3.7 p.p. by 2022. This settlement expansion corresponds with large and significant increases in mean night light radiance, highlighting the role of economic growth in stimulating land cover change. The settlement expansion also corresponds with descriptive evidence of Bangladeshi immigration and economic expansion in response to camp openings ([Filipski et al., 2021](#)). My results are robust to alternative specifications and are more pronounced in the areas near the Kutapalong Expansion Site.

To date, our understanding of how refugee camps influence environmental outcomes remains limited. There are two papers that use causal inference techniques to examine this question, and both focus on camps across sub-Saharan Africa (SSA). [Maystadt et al. \(2020\)](#) use low-resolution spatial tiles to examine changes in land cover attributes in response to camp openings. They find that the conversion from forest to agriculture rises after camps open, but the treatment tile's vegetation density marginally improves in response to camps. [Salemi \(2021\)](#) uses high resolution spatial data to examine forest cover responses to camp openings in areas directly adjacent to camps. She finds that refugee camp openings have no economically significant effect on forests across the subcontinent. Together, these studies suggest that while the agricultural agglomeration effect associated

²The harmonized product reports radiance in whole numbers, which can underrepresent variation in rural, lower-income settings where small changes matter.

with camps may be extensive, camps have little forest cover impact in their immediate vicinity.

But these findings may not be externally valid. Refugee camp areas in SSA tend to be characterized by high land availability and lower population densities. The muted local results may be explained by a sustainable supply of biofuel inputs for local communities and refugee populations. Cox Bazar provides us with an opportunity to consider a different context: one of high population density and binding land constraints.

The remainder of this paper is as follows. [Section 2](#) lays out the theoretical channels through which refugee camp establishment may affect land cover. It describes both the direct and indirect effects that may occur locally or regionally. In [Section 3](#), and in the framing sections that follow, I draw additional information from the Cox Bazar Panel Survey (CBPS) 2019 wave ([Baird et al., 2021](#)) to provide additional insight into the characteristics of the encampment region. Next, [Section 3](#) provides background on the Rohingya peoples, the 2017 displacement event, and the humanitarian response in Cox Bazar. [Section 4](#) introduces the land cover classification data I use in this study, describing all data cleaning and presenting descriptive changes over time. In [Section 5](#) I introduce the methodological approach, and I report findings from my main assessment, heterogeneity analysis, and robustness checks in [Section 6](#). I offer concluding remarks in [Section 7](#).

2 Refugee camps and land cover change

The topic of refugee camp-associated environmental change gained academic attention in the 1990s. Scholars at the time debated whether refugees are “exceptional resource degraders” due to their lack of land tenure, extreme poverty levels, and uncertainty regarding their time at a given location ([Jacobsen, 1994](#)). To date, there is no strong empirical evidence to support the idea that displaced people have characteristics that lead them to degrade landscapes faster than others ([Black, 1998](#); [Black and Sessay, 1999](#); [Kibreab, 1997](#)).

Instead, I propose a means of thinking about refugee-associated land cover change that manifests directly (due to refugee activities) or indirectly (due to changes in local

market demand). Indirect effects include that are expected to occur locally (in the area adjacent to the camp) and regionally (in areas relatively far from the camps).

The primary method through which refugees may directly affect local land cover is through NTFP extraction, including fuelwood and shelter materials. The latter will particularly be the case when humanitarian service providers do not supply refugees with shelter or energy inputs. While refugee activities may directly influence regional land cover changes in contexts of free mobility, this is unlikely to occur in Bangladesh, where refugees who arrived after 1992 do not have the right to leave encampment areas ([Section 3](#)). Indirect effects may manifest locally or regionally. The first indirect causal channel is related to economic growth. Refugees are consumers who leverage credit, savings, and wages (including income earned working, despite prohibitions) to consume in local markets. Refugees also sell portions of their in-kind aid basket to diversify consumption ([Betts et al., 2017](#)). Camp management (frequently overseen by UNHCR and the host government) is also labor-intensive, and jobs related to service delivery and security influence demand for native labor.

Camp-stimulated boosts in market demand have been demonstrated using nighttime lights ([Alix-Garcia et al., 2018](#)), and market assessments have revealed significantly higher prices for food items outside of the in-kind aid basket, a sign of increased demand mediated by humanitarian aid provision ([Alix-Garcia and Saah, 2010](#)). Descriptive results from the areas near Cox Bazar camps additionally provide evidence of increased business activity adjacent to camps ([Filipski et al., 2021](#)).³

In response to higher demand, increased economic production may come at the expense of local forest cover, which is drawn on as a production input or cleared to make way for brick-and-mortar establishments. Increased demand for food will likely lead to agricultural intensification. While augmented demand may influence forest-to-agriculture conversions close to the camps, results from [Maystadt et al. \(2020\)](#) and [Salemi \(2021\)](#) suggest that such conversions may take place at a regional level.

³Filipski and colleagues' survey data from business owners closer to and further from the Rohingya refugee camps found that 26% of Bangladeshi business owners operating on the periphery of the camps had started their business after the 2017 Rohingya large-scale arrivals. This is a considerably higher share than the authors find among Bangladeshi business owners further from camps, 10% of whom started their operations after August 2017.

The second channel through which refugee camps may indirectly affect land cover relates to in-migration. Job creation and economic activity may pull hosts towards camp areas, where they settle close to markets and jobs. [Filipski et al. \(2021\)](#) provides descriptive evidence that supports this theory⁴. Representative household data from the CBPS 2019 additionally shows a marginal increase in the share of the Bengali population near camps who arrived after the refugee population arrival ([Figure A1](#))

3 Background

3.1 The Rohingya people in Myanmar

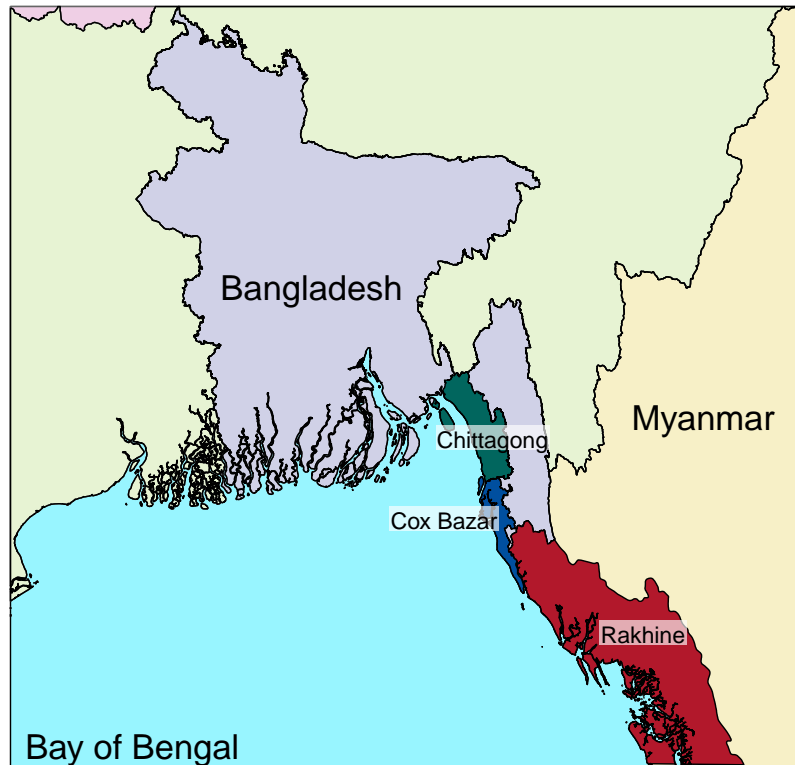
The Rohingya ethnoreligious group is a minority population from Myanmar concentrated in Rakhine State ([Figure 1](#)). Rakhine corresponds to the historic Arakan region, which the Rohingya people consider their homeland. The Rohingya population is predominately Muslim, are of Indo-Aryan ethnicity (like Bengalis), and their language is a variant of Bengali ([Blakemore, 2019](#)).

After Burma gained independence in 1948, the Rohingya people were considered citizens as part of an inclusive constitutional framework, though the Burmese national government largely sidelined minority groups from political leadership ([Farzana, 2017](#)). In, 1982 the Burmese Citizenship Law officially stripped the majority of the Rohingya of their citizenship, excluding the Rohingya minority from the taxonomy of ethnic groups considered citizens in Myanmar ([Farzana, 2017](#)).

Since independence, there have been multiple periods of large-scale Rohingya displacement from Myanmar. Secondary accounts usually focus on intense violence in 1978 and 1991-1992. In both episodes, tens of thousands of Rohingya refugees were forced to seek asylum in Cox Bazar ([Ullah, 2011](#)). While these moments of large population displacement garner considerable attention, smaller-scale displacement of Rohingya asylum-seekers to Bangladesh has also occurred rather continuously over time, as households faced violence, persecution, extortion, and forced labor at the hands of Myanmar's mili-

⁴The authors find that 8% of Bangladeshi business owners operating within or near camp areas had moved their residence to the camp periphery after August 2017.

Figure 1: Contextual map of Bangladesh



Notes: Map produced by author using publicly available spatial data of administrative divisions.

tary (the Tatmadaw) or aligned extremist groups (Human Rights Watch, 2000; Ibrahim, 2016).

It is difficult to estimate the population size of the Rohingya refugees in Cox Bazar at the eve of the 2017 displacements. Many of those who fled to Bangladesh in earlier years were repatriated back to Myanmar, in some cases only to be displaced again when conditions worsened (Ullah, 2011). From Bangladesh, others have fled to southeast Asia by sea (Aung et al., 2015). It is generally believed that about 200,000 Rohingya refugees resided in Cox Bazar - either in planned camps, makeshift camps, or among host communities - shortly before the most recent population influx (Parnini et al., 2013; Tay et al., 2018).

3.2 Cox Bazar, Bangladesh

Cox Bazar is a district in southeastern Bangladesh's Chittagong division (Figure 2). The district is not a particularly large area, at only about 213,639 ha (2,136.39 km²), roughly the size of the

US state of Rhode Island. Cox Bazar has a subtropical climate: its December-February dry season is followed by increasingly hot and wet temperatures, culminating in a summer monsoon period. The local terrain is best characterized as low-lying, hilly, and swampy. The district is known for its natural areas, with relatively high levels of forest cover and large swaths of the landscape designated as protected areas (national parks or wildlife sanctuaries). [Figure 2](#) shows the protected area locations in the district.

As of the 2022 Census, there are approximately 2.8 million residents of Cox Bazar, excluding those living in camps ([Bangladesh Bureau of Statistics, 2023](#)). The 2022 Census figures represent a 27% increase in the non-encamped population since 2011([Bangladesh Bureau of Statistics, 2014](#)). Excluding the encamped population, the current population density is on average about 1,300 persons per km².

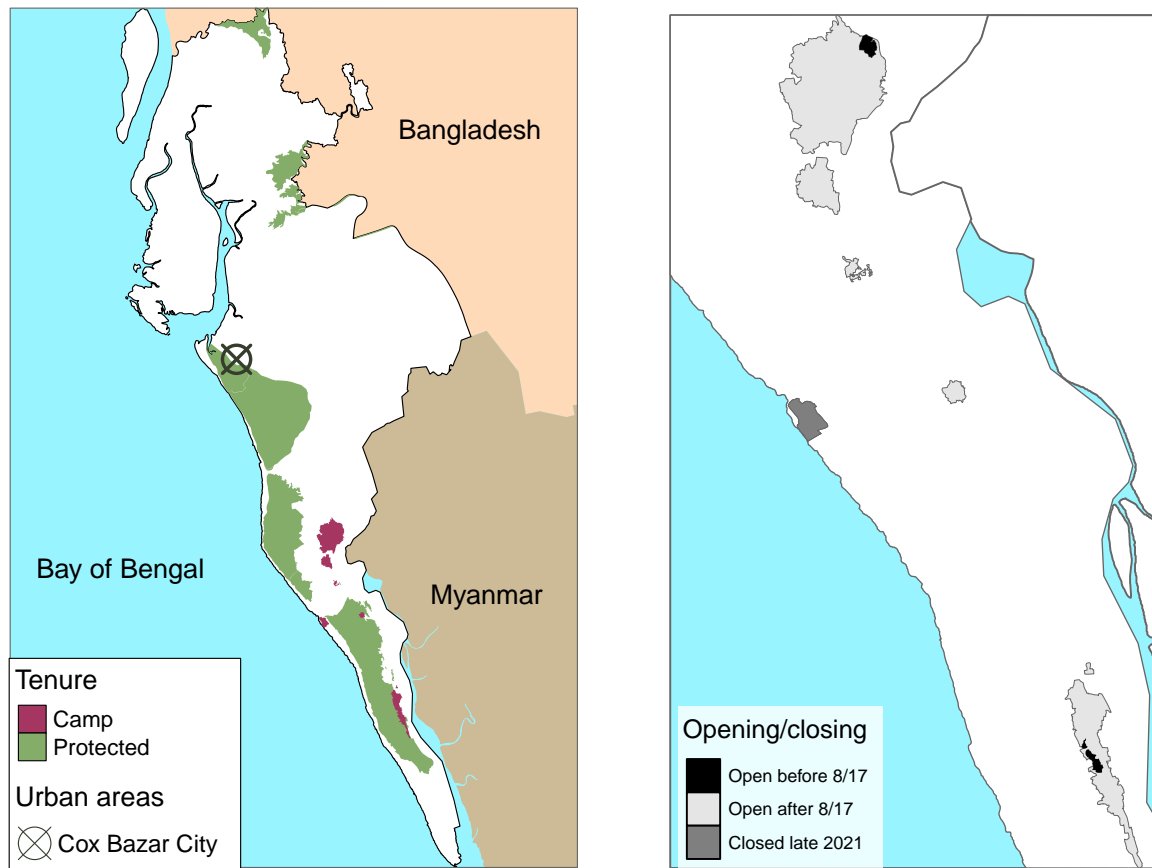
3.3 2017 displacement and emergency period

Violence targeting the Rohingya people began in 2016 and intensified in 2017. The UN human rights chief called the atrocities a “textbook example of ethnic cleansing” ([Nebehay, 2017](#)). After systematic review, the U.S. government concluded that during this period, the Tatmadaw and associated militias committed genocide ([Blinken, 2022](#)), and the United Nations Independent Investigative Mechanism for Myanmar concluded that the violence constituted a crime against humanity ([Human Rights Council, 2022](#)).

In October 2016, a militant group attacked three Myanmar border security posts in Rakhine State, and nine soldiers were killed (Reuters, 2016). Under the belief that Rohingya militias were responsible, the Tatmadaw launched a violent campaign against Rohingya villages. According to Amnesty International, the Tatmadaw and associated militias engaged in indiscriminate shootings and killings, rape, and sexual violence. They arrested hundreds of Rohingya men, mainly community leaders. Amnesty’s GIS analysis confirms that the military burned down hundreds of Rohingya homes. The Government of Myanmar additionally banned humanitarian aid from entering Rakhine State ([Amnesty International, 2016b](#)).

According to UNHCR, 74,000 Rohingya asylum-seekers sought refuge in Bangladesh between October 2016 and July 2017 ([Tan, 2017](#)). Human rights organizations monitoring

Figure 2: Maps of Cox Bazar with locations of camps, protected areas, and the capital city



Notes: Map on left produced by author using publicly available spatial data of administrative divisions, Protected Planet spatial data on protected areas, and camp boundaries provided by UNHCR and IOM’s Inter-Sector Working Group. Study area (shown in white) includes Cox Bazar district and adjacent Naikhongchari subdistrict in neighboring Bandarban district. Inclusion of Naikhongchari is covered in Section 4. Map on right shows camp areas and aggregates adjacent camps within the same “expansion site.” Camps in black existed prior to the 2017 arrival of refugees and are considered by the Bangladeshi government as “planned.” Camps in light grey were created after August 2017 and are considered by the government as “makeshift.” Camp 23 is filled in with medium grey: it opened in 2017 but closed late 2021 (Health Sector Coordination Team, 2021).

the situation reported that Bangladeshi border security sent many back to Myanmar, in violation of the principle of non-refoulement (Amnesty International, 2016a). Those who did get through the border sought refuge in existing refugee encampment areas. For our analysis, it is important to note that this involuntary migration took place during the time window of our 2017 dry season (February) land cover composite (Section 4). But since refugees self-settled near existing camps, any land cover modifications would likely have taken place within the interiors of the later-established encampment areas. This helps to assuage concerns about temporal misclassification within the identification strategy.

On August 24th of 2017, militants attacked 30 border posts in Rakhine State and killed 12 security officers. The Arakan Rohingya Salvation Army (ARSA) claimed responsibility (Reuters, 2017). In retaliation, the Tatmadaw and affiliated militias launched another campaign of violence against Rohingya civilians, with widespread arson, killings, and sexual violence (International, 2017). Estimates of the number of Rohingya people killed after the August border attacks range from 9,000 to over 20,000 people (Jakes, 2022; Mohshin Habib, 2018). This period of violent persecution triggered a much larger movement of asylum seekers across the border. Between August 2017 and January 2018, UNHCR population monitoring suggests that approximately 688,000 Rohingya asylum-seekers crossed the border into Bangladesh (UNHCR, 2018a). In May of 2018, UNHCR estimated the entire Rohingya refugee population in Cox Bazar at 886,788 people, including 720,849 refugees who had arrived since August 2017 (UNHCR, 2018c).

Thousands of the earliest arrivals sheltered in or near pre-existing camp areas, putting pressure on services. Many thousands more sheltered in areas nearby existing camps or briefly lived alongside host communities. By October 6th, the Government of Bangladesh (GoB) had already allocated 2,000 acres of land west of the existing Kutapalong Refugee Camp for new encampments (UNHCR, 2017d). This designated land largely corresponds with a large share of the location of the Kutapalong Expansion Site as it exists today (Figure 2). Following this land designation, the GoB military cleared the land for human settlement and constructed access roads. As of October 2017, these 2,000 acres were expected to accommodate half a million refugees. The GoB allocated additional land for camp areas over time (UNHCR, 2018b), but overcrowding in camps has persisted.

Humanitarian partners immediately mobilized but struggled to keep up with soaring demand for emergency assistance. Over the course of just a few months, agencies rapidly registered thousands of asylum-seekers as refugees, installed hundreds of tube-wells, constructed thousands of latrines and water hand-pumps (UNHCR, 2017c), distributed thousands of tarpaulins (UNHCR, 2017d), developed emergency health supports to combat diarrhea and malnutrition (UNHCR, 2017b), distributed critical food supplies, and rapidly planned settlement areas in newly designated camps. Despite considerable

effort, UNHCR documentation acknowledges that many refugees remained out of reach of emergency assistance during these months (UNHCR, 2017a).

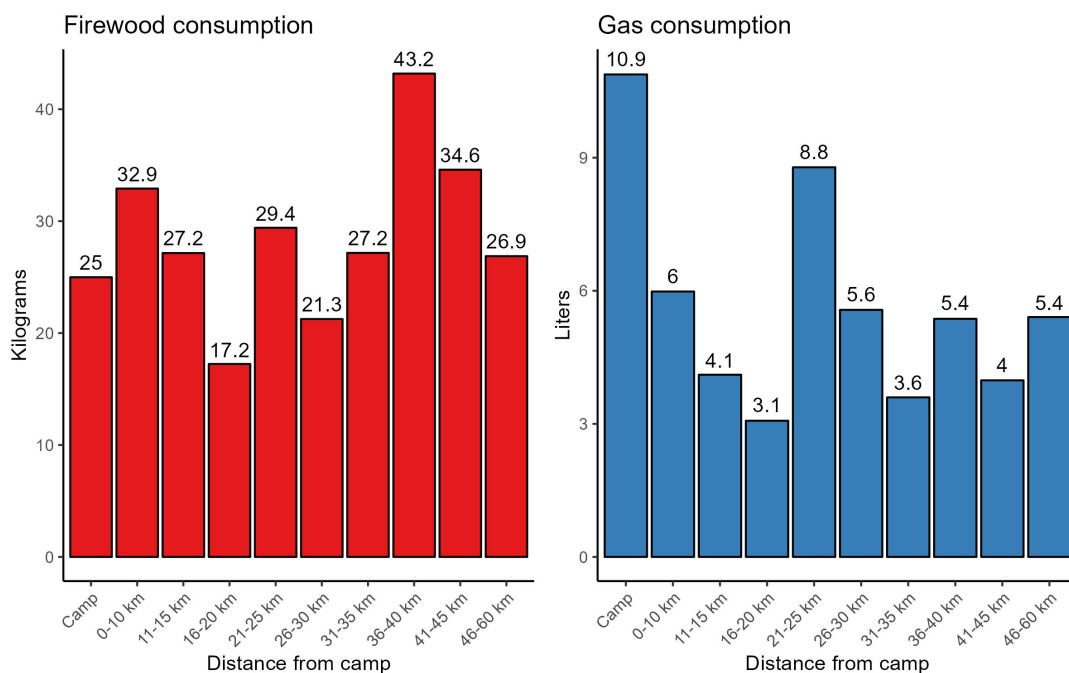
3.4 Refugee hosting 2017 and after

Between 2017 and 2018, the areas designated for encampments were increasingly modified for human settlement. During the study period, the overall complex came to be made up of 35 distinct camps, many of which are clustered together (Figure 2). These camps are now the most overcrowded in the world. On average across all camps, the population density is approximately 33,000/km², which matches the density of Bangladesh’s capital, Dhaka⁵. As of 2019, the Kutapalong expansion site had a population density of 43,000 people per km². Many of the camp areas are close to or even overlapping with protected areas, including Inani National Park and the Teknaf Wildlife Sanctuary (Figure 2).

Aside from a very small number of refugees who arrived prior to 1992 and live in existing, “planned” camp areas or among host communities, the overwhelming majority of the newly arrived population (and those who sought refuge between 1992 and August 2017) have limited protected status (Filipski et al., 2021). Many are registered with UNHCR, protecting them against *non-refoulement* and ensuring their access to humanitarian services. But the GoB has not registered refugees since 1992 (UNHCR, 2007), and without national recognition, refugees such as the 2017 arrivals cannot legally work or own property, and they are legally prohibited from leaving camp areas. I assume that these restrictions are imperfectly enforced, meaning refugees had limited access to peripheral areas. I also assume that enforcement of mobility restrictions rose over time: security checkpoints have emerged along camp boundaries, and fencing construction around camp boundaries began in 2019. By 2020, much of the Kutapalong expansion site was enclosed by barbed wire fencing (Fortify Rights, 2020). CBPS 2019 data suggests that the majority (98%) of all Rohingya people in Cox Bazar are living in a camp (Table A1).

⁵Using camp boundary data from the Inter-Sector Coordination Group (ISCG), I estimate the land area of the encampments (as of 2020) at 25.5 km². The CBPS 2019 data suggests that 98% of Rohingya refugees in Cox Bazar are living in camps (Figure A1). In July 2020, the Rohingya refugee population of Cox Bazar was estimated at 860,494 people (UNHCR, 2020). Assuming 98% of these refugees are in camps, this means that in 2020, the average population density across all camps was approximately 33,000 per km². The population of Dhaka in 2022 was 10,278,882 people, and the city size is 306.4 km² (Bangladesh Bureau of Statistics, 2022). This results in a 2022 population density estimate of about 33,500 per km².

Figure 3: Average energy consumption in previous week by energy type and distance to the nearest camp, CBPS 2019



Notes: Weighted averages (household weights) compiled by study team using Cox Bazar Panel Survey (CBPS) 2019 data. Distance to nearest camp is based on non-linear travel distance. Study team converted various units of measurement for firewood and LPG gas into kg and liters, respectively. Because 98% of Rohingya refugees live in camp areas and very few Bangladeshis live within camp boundaries, observations within camps can be assumed to be refugee observations and out-of-camp observations reflect the consumption of non-refugees.

UNHCR and its partners have made considerable efforts to address cooking fuel demand in the camp areas. As early as November 2017, UNHCR began distributing crop residues to households for use with traditional stove technologies (UNHCR, 2017a). In late 2018, UNHCR launched an ambitious improved cooking technology drive. By December 2019, 112,188 households in refugee camps received a liquid petroleum gas (LPG) stove (UNHCR, 2019). Household data from 2019 demonstrates the stove rollout’s impacts on energy consumption (Figure 3). Gas consumption is the highest among households within refugee camps (10.9 liters in previous 7 days). Areas near camps exhibit declining consumption of LPG energy, which speaks to limited efforts by UNHCR and its partners to deliver stoves to host households. Despite the high amounts of LPG usage in camps, firewood consumption remains an important source of fuel among encamped households. Past energy profiling suggests that households still consume firewood to satisfy energy demand when their LPG canisters run out of gas, which often occurs before the household is eligible for a free refill (UNHCR and WFP, 2021).

For encamped refugees, most gas consumption comes from in-kind transfers. And as of 2019, a large share (65%) of the firewood refugees consumed was acquired in markets (Figure A2). But refugees still extract firewood from the landscape, with 28% of fuelwood consumption obtained from harvesting. The share of firewood sourced from the landscape may have fallen since 2019, given the construction of fencing. Outside of camps, however, the share of firewood extracted from the landscape was considerably higher (57% in areas within 15 km travel distance from camp boundaries, and 66% in areas 16-20 km from camps).

Descriptive evidence points to a marginal increase in Bangladeshi in-migration near camps after their opening. The CBPS 2019 data suggest that 9 percent of Bangladeshis living 0-10 km travel distance from a camp boundary settled in the area after August 2017 (Figure A1). Between 10 and 25 km from the nearest camp, the percent of Bangladeshis who arrived after the 2017 declines. These statistics mirror findings in Filipinski et al. (2021).

4 Data

My analysis of land cover impacts uses the Dynamic World (DW) 10m resolution land-use land cover global data product. Dynamic World estimates the probability that a given 10-meter grid-cell is classified by one of the following classes: water, trees, shrubs, grasses, built-up, flooded vegetation, crops, bare, or snow and ice. The highest probability type is then selected as the prediction as the discrete, or “hard” classification. Researchers have evaluated the reliability of the hard classifications, scoring Dynamic World’s global accuracy at approximately 74% (Brown et al., 2022). Further evaluation indicates that forest (“tree”) cover is identified with about 81% accuracy (Venter et al., 2022), while settlement detection performs well overall but varies substantially between urban (80%) and rural (56%) areas.

These accuracy assessments are based on a hard classification approach, where each 10-meter grid cell is assigned solely to its dominant land cover class. To improve accuracy in rural settings with small and dispersed structures, I instead use Dynamic World’s probability layers. Rather than discarding subdominant signals as in a hard classification,

the probabilistic approach preserves information about mixed or transitional land cover, such as small shelters located alongside bare ground or cropland.

For each year 2016-2023, I use all Dynamic World layers available during the month February (the dry season, when cloud coverage is minimal) to generate a mean composite of each probability layer. I then upscale each 10-meter raster to 30 meters to reduce data volume and computational load⁶. The resulting object contains 2,899,227 grid-cells that form the basis of my sample.

I use additional geospatial data for the analysis. First, Protected Planet's World Database of Protected Areas provides information on which areas of Cox Bazar are designated as wildlife refuges or national parks (UNEP-WCMC and IUCN, 2021). I also use camp boundary data provided by UNHCR and IOM's Inter-Sector Coordination Group (ISCG, 2018) to determine camp proximity.

I additionally draw on nighttime light radiance data, an increasingly popular proxy of economic productivity and public investment (Bruederle and Hodler, 2018; Martinez, 2022). Specifically, I use the VIIRS 500m annual composites 2013-2021 Version 2.1, which have been cleaned of spurious noise⁷ and provide a depiction of stable nighttime light radiance over time. The data are scaled from a value of 0 to 63, where 0 represents no detectable light while 63 corresponds with the planet's brightest core urban areas.

Using the grid-cells of the upscaled Dynamic World layers, I generate a tabular sample where each unit represents one 30-meter grid-cell. For each unit, I find the corresponding probability of each land cover class for each year (2016-2023). I determine each unit's Euclidean (linear) distance to the nearest camp boundary, dropping the 27,737 grid-cells that fall within a camp boundary. I also intersect each grid-cell with the Protected Planet data to designate which fall within a protected area. Additionally, I construct a larger spatial matrix (1km resolution) and identify the intersection of each sample grid-cell with this larger grid. I use these intersections for my matching identification strategy and for clustering standard errors⁸.

⁶I unfortunately cannot obtain other monthly composites due to cloud cover obstructing significant areas of the study area

⁷For example, aurora, cloud cover, sunlight contamination, and various outliers are masked out of each year

⁸Clustering is intended to account for serial autocorrelation in spatial data while using a large data sample. The traditional approach to accounting for serial spatial autocorrelation in the error term is to use spatial regression tools, namely nearest neighbor matching. This method, however, is computationally intensive, as it requires working with an NxN nearest neighbors matrix.

Table 1: Land cover characteristics by year and proximity to camp boundary

	Year							
	2016	2017	2018	2019	2020	2021	2022	2023
Panel A: Whole sample								
Protected	0.143							
Forest	0.339	0.346	0.329	0.329	0.333	0.338	0.324	0.319
Vegetation	0.137	0.136	0.136	0.136	0.133	0.128	0.131	0.128
Agriculture	0.112	0.139	0.140	0.132	0.139	0.134	0.132	0.149
Bare	0.056	0.047	0.046	0.048	0.053	0.049	0.049	0.050
Settlement	0.053	0.083	0.100	0.099	0.088	0.100	0.112	0.111
Flooded veg	0.063	0.069	0.071	0.075	0.063	0.070	0.067	0.059
N	2,871,490							
Panel B: 0-5 km from camp boundary								
Protected	0.352							
Forest	0.410	0.411	0.372	0.362	0.382	0.387	0.372	0.377
Vegetation	0.148	0.147	0.153	0.151	0.141	0.133	0.137	0.131
Agriculture	0.130	0.123	0.127	0.123	0.135	0.121	0.121	0.128
Bare	0.048	0.042	0.043	0.044	0.046	0.042	0.045	0.043
Settlement	0.055	0.072	0.097	0.105	0.090	0.112	0.123	0.121
Flooded veg	0.061	0.064	0.063	0.066	0.058	0.060	0.057	0.054
N	390,285							

Notes: Observations are 30m grid-cells. Dynamic World land cover data represents probability of a given land cover class on the grid cell and is derived using mean composite from February layers for each year. Distance to nearest camp based on Euclidean distance function. Grid-cells within camp boundaries are excluded. “Protected” represents the proportion of the sample that is in a protected area. All time-varying land cover classification statistics represent the probability of a given class in the reference year.

Table 1 reports descriptive statistics for the sample collected from the entire study area (excluding camp interiors) as well as the areas 0-5 km outside of camps. I also map forest and settlement data for 2017 and 2020 in Figure 4, and the Appendix includes the equivalent map for vegetation and agricultural cover (Figure A5). As shown in Table 1, 15% of the province falls under a protection mandate, and the percent of protected area is even higher in the 0-5km vicinity of camps (35.2%). Forest cover is the most common land cover class. Interpolating probabilities in Dynamic World as indicators of percentage cover, the data suggest that in 2016, 33% of the district, and 41% of the camp vicinity areas, were forested. The high forest cover near camps may be related to the relatively larger share of protected areas: considering the location of parks and refuges (see Figure

2), it is clear that forest cover is more dense in the protected areas of the district before and after camp opening (Figure 4).

The descriptive statistics in Table 1 show a four percentage point reduction in forest cover between 2017 (pre-camp openings) and 2018 (post-openings) within the camp vicinities. Without the counterfactual, however, it is unclear if a loss of this extent would have occurred in the absence of the camps. My identification strategy, described in the next section, provides the causal estimates.

Across the district and in the camp vicinities, vegetation (shrubs and grasses) and agricultural cover are relatively less common, at about 11-15%. Vegetation appears evenly dispersed throughout the district (Figure A5), while agricultural cover tends to manifest in proximity to settled areas (Figure 4). These classes does not appear to change meaningfully over the time series, but given their relative magnitudes and the potential impacts of camp opening on these classes, I include them in my analysis.

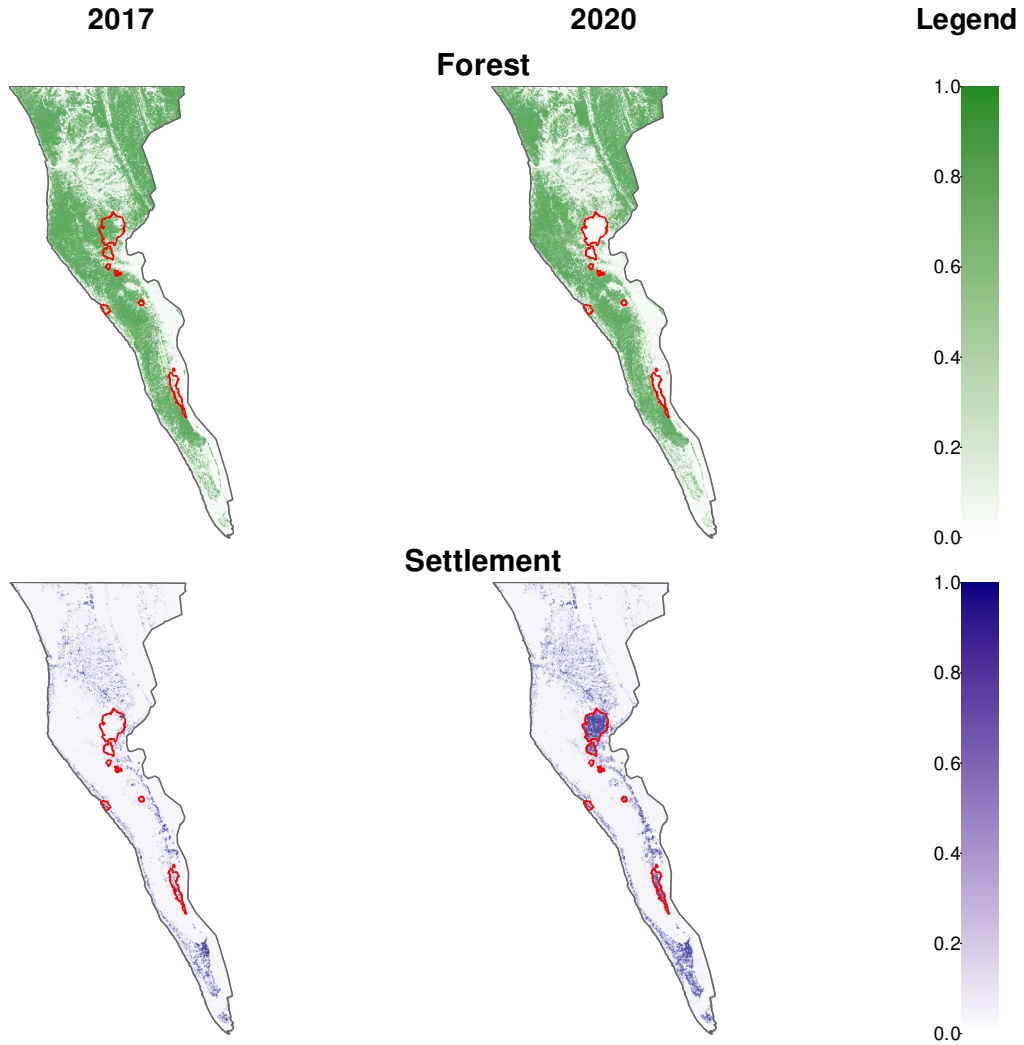
Cox Bazar is predominately rural, so the low settlement density is not surprising. But across the province, settlement is expanding over the time series, from 5% in 2016 to 11% in 2023. The settlement expansion is particularly pronounced near camps, which went from about 7% settlement cover to 12% between 2017 and 2018. The changing gradient is subtle but visible in Figure 4. Settlement cover impacts can speak to both in-migration and economic expansion in response to camp openings, both of which may impact the landscape. And since settlement is expanding throughout the district, a robust identification strategy is necessary in order to attribute these changes near camps to camp opening. Hence, I include settlement cover in my analysis.

Bare ground and flooded vegetation cover are not particularly common in the area and do not vary considerably over the time series. I omit these categories from my analysis.

5 Method

My analysis focuses on areas 0-5 km from camp boundaries to isolate the local effect of encampment on nearby land cover. Prior research suggests that the agglomeration effects of camps typically manifest within 4–10 km of their borders (d’Errico et al., 2022; Taylor et al., 2016). Given concerns about direct refugee-driven degradation of surrounding

Figure 4: Probability of forest and settlement cover by year in and near camps



Notes: Author's production using Dynamic World probability of land cover data derived using mean composite from February layers for each year. Camp boundaries sourced from UNHCR and IOM Inter-Sector Working Group.

landscapes, I also expect damages to depend on foraging access costs, which rise sharply over hilly terrain traversed on foot. Defining my treatment area within the buffer 0-5 km buffer captures the zone where the agglomeration effect is expected and where foraging costs are lowest.⁹ To avoid contamination of my control sample, I omit observations at distance $d \in (5, 20]$ km from the nearest boundary.

Refugee camp locations are not randomly determined (Maystadt and Verwimp, 2014; Salemi, 2021), necessitating a methodological approach that provides valid counterfactual estimates. My analysis combines a matching method with a difference-in-differences

⁹A careful study of the extent of the agglomeration effect is beyond the scope of this study.

framework, a technique that can improve on the representativeness of counterfactual estimation relative to the use of DID or matching in isolation ([Heckman et al., 1997](#); [Roth et al., 2023](#); [Smith and Todd, 2001](#)).

Because of autocorrelation in the spatial data, and particularly in the treatment group, I aim to avoid matching an assortment of non-adjacent 30m grid-cells from across the study area. Hence, I modify the approach to ensure that the matched samples represent clusters of contiguous grid-cells. To do so, I first upscale the 30m data to 1km resolution, computing mean probabilities. I then match the 1km treatment sample to 1km areas located $> 20\text{km}$ from the nearest boundary and positioned anywhere in the study area. I specifically match on the probability of forest, settlement, vegetation, and agricultural cover in 2016 and 2017 as well as the share of the 1km grid within a protected area.

For my matching procedure, I estimate propensity scores using a probit regression model and compute inverse probability weights to assess covariate balance. To construct the matched sample, I implement nearest-neighbor matching with one control per treated observation ($k = 1$) and impose a strict caliper of 0.1 on the propensity score to ensure close matches. I exclude observations falling outside the region of common support. Observations that fall in the matched 1km grids constitute my estimation sample. I report detailed information on covariate balance and the locations of matched observations in [Appendix Section B](#).

I expect the treatment effects to evolve over time, meaning that averaging across the full study period could obscure important dynamics. For instance, if interventions such as camp fencing or improved cookstove rollouts later reduced pressure on surrounding landscapes, slowing deforestation or enabling forest recovery, then a simple average across years would understate the magnitude of deforestation impacts that occurred before these changes. Likewise, camp-stimulated settlement or agricultural expansion may not occur within the first period, but may instead intensify over the years. For this reason, my analysis uses the matched counterfactual sample to estimate the following difference-in-differences event study:

$$Y_{it}^c = \sum_{s \neq 2017} \beta_s^c T_i \times \text{Year}_s + \tau_t + \omega_i + \varepsilon_{igt} \quad (1)$$

In the regression above, 2017 serves as the base year¹⁰. Outcome variable Y_{it}^c represents the probability that grid cell i in period t is land cover class c . For each class, I regress this outcome on the set of interactions between observation each observation year $s \in \{2016, 2018, \dots, 2023\}$ and a boundary indicator for whether the observation is 0-5 km from a camp boundary $T_i = 1\{d_i \in [0, 5]\}$.

I include year and unit fixed effects. The grid-cell fixed effect accounts for a variety of time-invariant characteristics important for the study, such as soil fertility, whether the pixel is in a protected environmental area, proximity to main roads, and steepness of the slope. Given the small geographic scope of this study, the time fixed effect controls for inter-year variations that are plausibly homogeneous across the district, such as annual rainfall. I also cluster standard errors using each unit's intersection with the previously discussed 1km grid g ¹¹.

The event study provides one pre-treatment trends estimate for 2016-2017. Given matching, the pre-trend should be close to zero to offer support of the satisfaction of the parallel trends assumption. The temporal scope of the pre-treatment data, however, limits the robustness of the pre-trends test. Throughout, my identifying assumption is that the 2016-2017 differences in trends between treatment and matched control reflect the differences in trends in earlier years for which we do not have Dynamic World data.

In the following sections I describe my heterogeneity analysis, robustness checks, and assessment of mediating factors. Note that each procedure relies on a newly matched sample. Whenever the scope of the treatment group or control group is modified, matching is repeated prior to event study estimation.

¹⁰Although the large population influx occurred in August 2017, my use of February Dynamic World layers ensures that 2017 constitutes the final pre-treatment period. See [Section 3.3](#)

¹¹Because there is no clear group structure to the observations ([Cameron and Miller, 2015](#)) and because I am not using two-stage sampling ([Abadie et al., 2023](#)), it is unclear whether clustered standard errors are necessary. [Bertrand et al. \(2004\)](#) argue that within a DID framework, standard errors must be clustered at some group level to avoid misleadingly small standard error estimates. Moreover, serial autocorrelation of the error term is likely between geographically neighboring grid-cells. Given this serial autocorrelation, I cluster standard errors based on the sample grid-cells intersection with a 1km matrix of grid-cells

5.1 Heterogeneity analysis

Given the importance of protecting forest cover and biodiversity near camps, I conduct a heterogeneity analysis to see if pixels in protected areas are deforesting more or less than pixels in non-protected areas. I use the matching procedure to draw a new counterfactual sample using protected area grid-cells only. These protected grid-cells within 5km of the nearest camp primarily fall in Inani National Park and the Teknaf Wildlife Sanctuary.

There are numerous camp areas across the southern half of the Cox Bazar, but the Kutapalong Expansion Site stands out for its population size and density. It is now considered the largest refugee camp in the world. Given potentially larger effects near the Kutapalong Expansion Site, I repeat the analysis omitting all grid-cells that are 5 km below the southernmost extent of this area and identifying exposure based exclusively on a grid-cell being within 5km of the Kutapalong Expansion Site boundary¹². I again repeat the matching procedure to generate a unique counterfactual group for this estimation.

5.2 Robustness checks

A potential threat to identification relates to the scope of the impact. Given the scale of the displacement event, the large influx may have changed land use patterns across Cox Bazar, contaminating the counterfactual pool. I therefore perform a robustness check in which I sample the Chittagong district, a coastal administrative division directly north of Cox Bazar, for my counterfactual sample (see [Figure 1](#)). After matching, I re-estimate my primary event study specification with the area 0-5 km from the nearest camp serving as control.

My results may also be sensitive to the definition of the treatment group. As mentioned, past research finds that the agglomeration effect of a refugee camp may reach up to 10km outside its boundary. I therefore repeat the matching procedure from my primary specification, but instead of defining the treatment group as being 0-5 km from the nearest camp, I use grid-cells 0-10 km from the nearest camp.

¹²Specifically, I use the pre-2017 Kutapalong Refugee Camp as well as Camp 1 (E, W, X), Camp 2 (E, W), Camps 3-7 (including the Camp 4 extension) Camp 8 (E and W), Camp 9-19, and the Camp 20 series (Camp 20, its extension, and Camp 20 C).

Finally, I re-estimate the primary results omitting the Naikhonchari subdistrict of neighboring Banderban. I include this subdistrict in my primary specification because of its spatial adjacency with the Kutapalong camp complex (see [Figure A3](#)). But Banderban and the Chittagong Hill Tracts have a long history of conflict, and to this day, there is a strong military presence throughout the district ([Chittagong Hill Tracts Commission, 2000](#); [IWGIA et al., 2012](#)). Given the ongoing militarization of Banderban, camp proximity impacts may be more muted there despite proximity.

5.3 Mediating factors

A fully comprehensive mediation analysis is unfortunately beyond the scope of this study. In particular, analyzing the role of two relevant interventions - the rollout of LPG cookstoves to Rohingya refugees and some local Bangladeshis, and the enclosure of the camps in wire fencing - requires additional information on the location of these rollouts over time. I examine how forest trends align with secondary information on these interventions and speculate on potential impacts.

I can more thoroughly examine evidence of economic growth playing a role in the land cover results. To do so, I replicate the primary analysis using the VIIRS 500m nighttime lights data 2012-2020. Because VIIRS has a coarser resolution than my primary sample, and because averaging over an even larger grid will further muddle the already limited variation in a nighttime lights product across a rural landscape, I perform matching on the 500m sample itself. Given the coarser resolution, I cluster standard errors using a 2km grid instead of a 1km grid. And because VIIRS represents an annual composite, I use the 2016 year as my baseline instead of 2017¹³.

6 Results

For my main findings, as well as my heterogeneity analyses, robustness checks, and mediation analysis, I report full regression results in [Appendix Section C](#). Evaluations for each matching procedure are in [Section B](#).

¹³The 2017 year may contain imagery from after the August 2017 influx. To ensure that the pre-treatment period is not contaminated with post-treatment observations, I therefore use 2016.

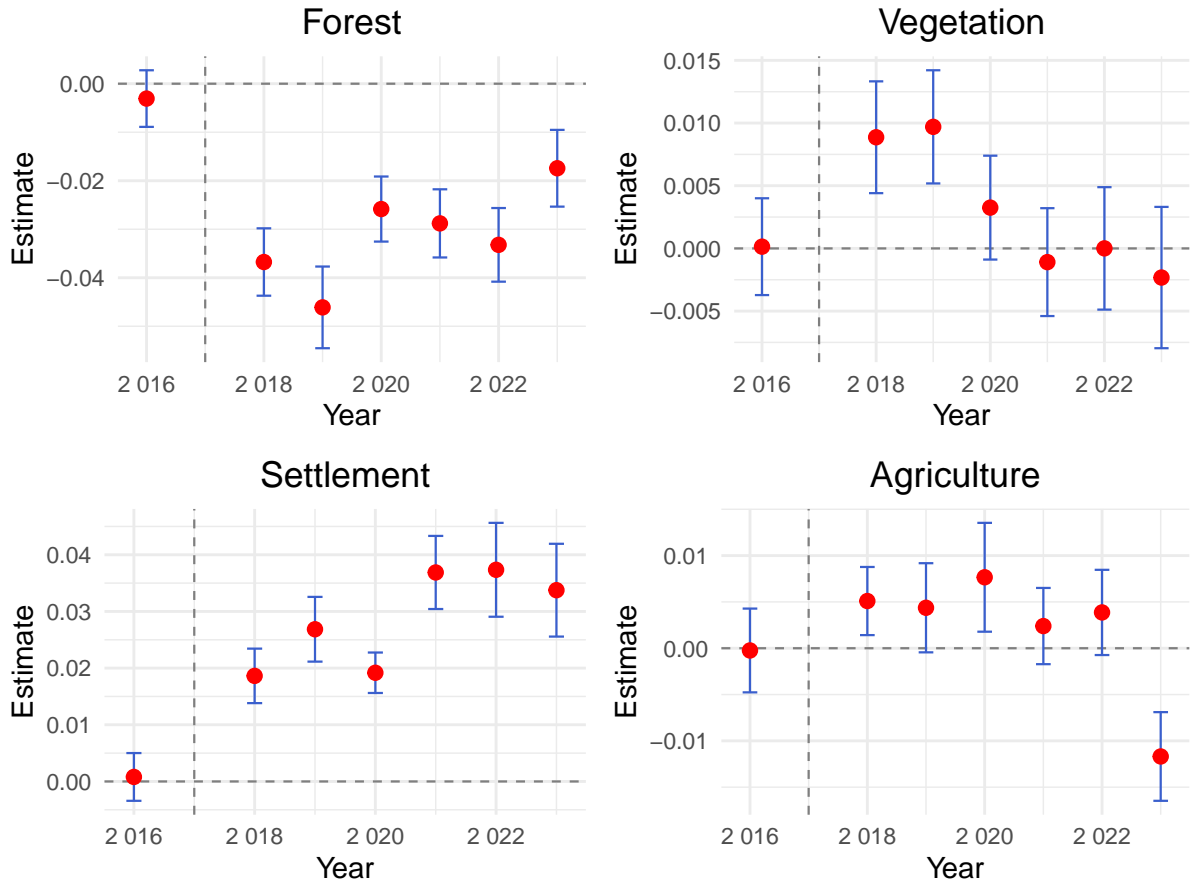
Matching for my primary analysis yields a sample of 347,561 30m comparison grid-cells and 305,213 treated grid-cells¹⁴. Matching substantially reduces covariate imbalance, bringing the absolute standardized mean differences below 0.1 for all variables and close to zero in most cases (Figure A6). Balance tests reveal differences that are very small in magnitude (Table A2). T-tests suggest that these small differences are statistically significant, but this is likely attributable to the very large sample size. Moreover, for the difference-in-difference framework, a significant difference in one period does not violate the identification strategy so long as the trends are not significantly dissimilar. Mapping the matched comparison sample (Figure A7), I find that the procedure selects areas 20-40 km from the camp boundaries, with fewer observations drawn from the northernmost area of the district. Because I include the protected area status in matching, a large share of the matched area is drawn from the Himchari National Park.

Figure 5 illustrates the primary event-study results (full estimates reported in Appendix Table A15). The estimated pre-treatment trend (2016–2017) is close to zero and statistically insignificant across all four specifications, supporting the parallel trends assumption. Following the August 2017 refugee arrival, the probability of forest cover within 0–5 km of camp boundaries declines sharply, particularly during the first two years. The magnitude of forest loss peaks in 2019, when forest cover is 4.6 percentage points (p.p.) lower than at baseline, representing a 12% reduction relative to the matched sample mean (Table A2).

By 2020, forest cover in the treatment area begins to recover, with losses relative to the 2017 baseline narrowing to 2.6–3.3 p.p. between 2020 and 2022. Because tree regeneration typically requires substantial time, the immediate rebound likely reflects a slowdown in deforestation rather than true regrowth. It may indicate that forest loss in the control areas began to marginally outpace that in the treated areas. The difference is smallest in 2023 (1.7 p.p.), a marked shift from the prior year. While this sudden decline in the cumulative effect could reflect random variation or measurement noise, it may also capture early signs of regrowth from fast-growing native species such as bamboo.

¹⁴Because I match on the 1km grid that the 30m grid-cells intersect, the treatment and control groups are not the same size. For example, some of the 1km matched grids in the treatment group intersect camp boundaries, and I drop all 30m grid-cells within the camps.

Figure 5: Event study results by outcome variable, Primary specification



Notes: Estimates of Equation 1, with 2017 as the reference year and 2016 coefficient representing the pre-treatment trend. Observations are 30m grid-cells. Outcome variable is the probability of a given land cover class on the grid cell and is derived using mean composite from Dynamic World February layers for each year. Treatment areas are 0-5 km from nearest camp boundary and are based on the Euclidean distance function. Areas > 5 km and ≤ 20 km from nearest camp boundary are omitted. Analysis uses propensity score matching to match 1km treatment and control gridcells based on pre-treatment and time-invariant observations. 30m observations within the matched 1km gridcells are used in the event study estimation. Standard errors clustered by 1km cluster grid.

Settlement cover also responds to camp openings, with evidence of continual settlement expansion over the time series. By 2023, the probability of settlement cover increases by 3.4 p.p. This represents a massive 44% increase relative to the matched sample at baseline. Settlement expansion does not follow the same pattern as forest cover loss, suggesting that a direct forest-to-settlement conversion is not driving the results. But expansions in settlement will leave less space for forest cover to return. Because Rohingya refugees who arrived 2017 or later are legally prohibited from residing outside of camps (as shown in descriptive data, see [Figure A1](#)), these settlement expansions may speak to the economic impact of refugee hosting, resulting in local growth and in-migration. I examine this further in [Section 6.3](#).

Results for vegetation and agriculture are notably more muted. Vegetation cover appears to rise in the first two years of hosting: this is likely due to tree loss, with less-valuable vegetative cover remaining on the previously forested pixel. Impacts on agriculture are very small in magnitude, switch sign over the time series, and are often insignificant or weakly significant. Agricultural cover is notoriously difficult to predict, especially during the dry season (February) when the spectral signatures of crops aren't easily detectable. Given these data limitations, my results for agriculture are inconclusive.

Given the significant and dynamic trends for forest and settlement, and the more muted results for vegetation and agriculture, the remainder of my analysis focuses on settlement and forest cover. Full results for all four classes are available in [Appendix Section C](#).

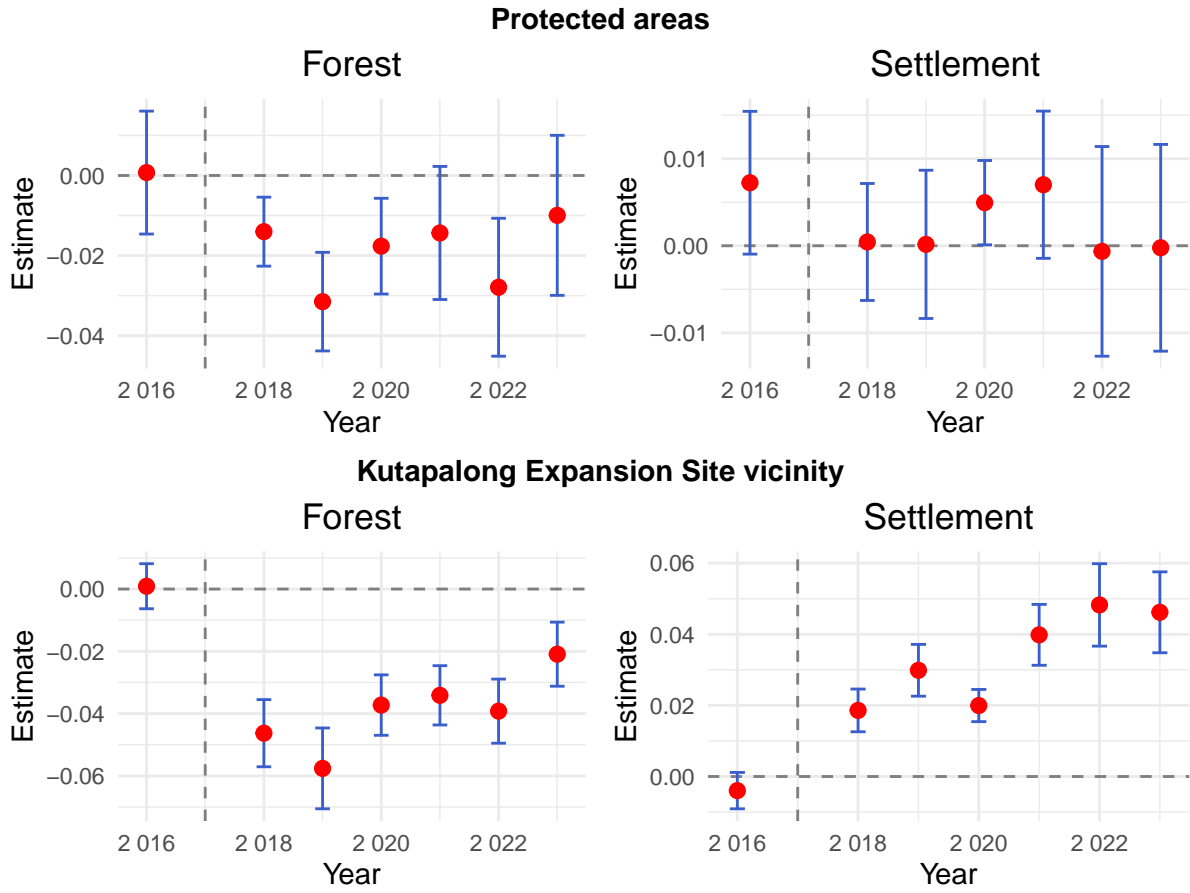
6.1 Heterogeneity analysis

[Figure 6](#) reports estimation results restricted to either protected areas or the vicinity of the Kutapalong Expansion Site, omitting all grid cells located more than 5 km south of the camp boundary.

Within protected areas, matching substantially improves covariate balance overall and particularly for forest cover ([Figure A8](#)). The matched counterfactual group is largely drawn from Himchari National Park, with a smaller share derived from small protected areas further north in the district ([Figure A11](#)). Estimation results suggest that forest losses may have taken place in protected areas within 5 km of camp boundaries, but these impacts were short-lived. Impacts are again largest in 2019 (3.2 p.p.) but attenuate immediately after.

Matching for the Kutapalong Expansion Site produces closely aligned propensity scores, though the absolute standardized mean differences for forest and settlement cover remain sizable ([Figure A10](#)). Pre-treatment trends, however, are still insignificant and very small in magnitude. The post-treatment event study results suggest that the impacts on settlement and forest cover are more acute in the Kutapalong vicinity. In this region, I measure 2019 forest losses as 5.8 p.p. (compared to 4.6 p.p. in the primary specification).

Figure 6: Event study results for forest and settlement cover, Results for protected areas and Kutapalong Expansion Site vicinity

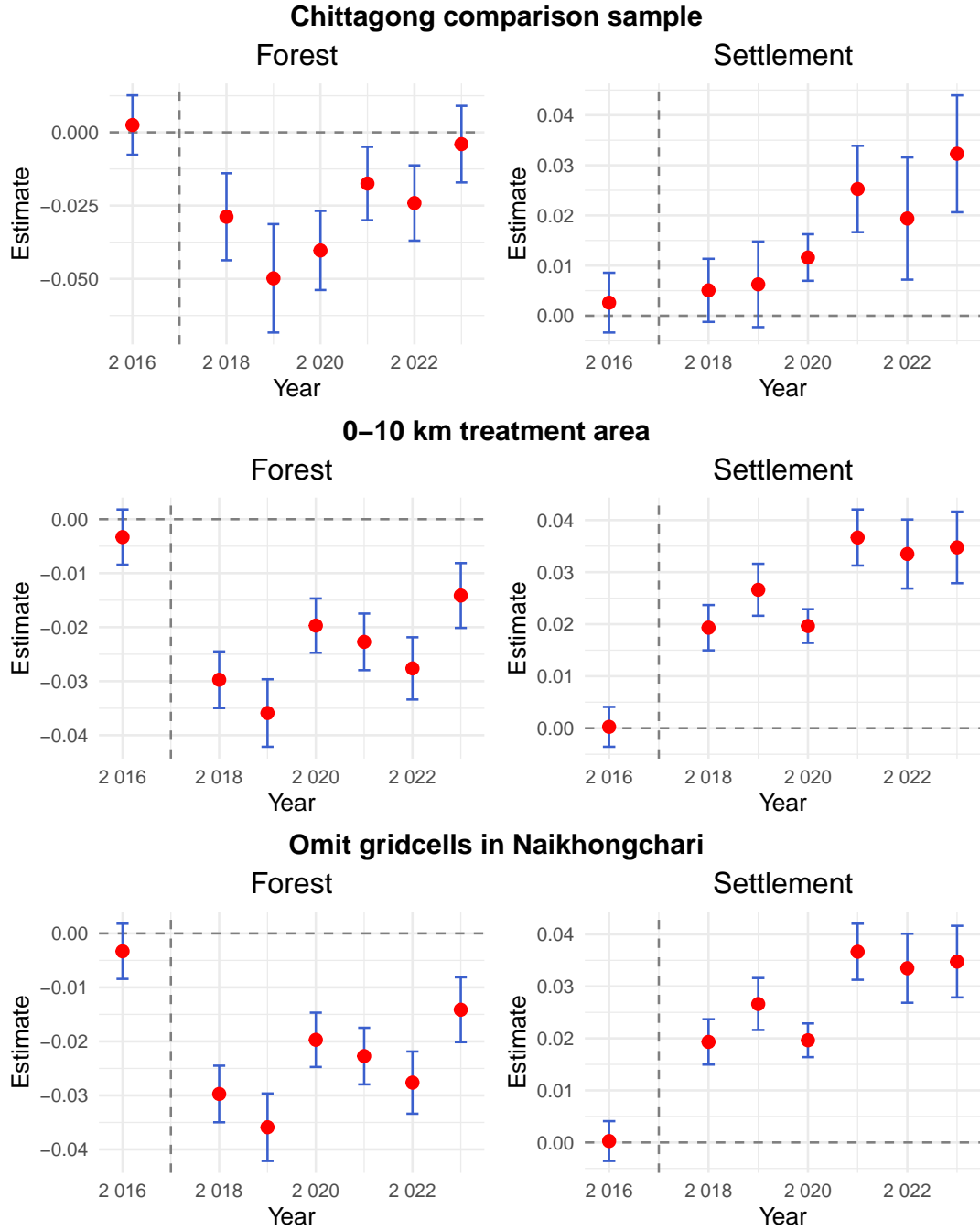


Notes: Estimates of Equation 1, with 2017 as the reference year and 2016 coefficient representing the pre-treatment trend. Observations are 30m grid-cells. Outcome variable is the probability of a given land cover class on the grid cell and is derived using mean composite from Dynamic World February layers for each year. Top row displays results for sample restricted to protected areas. Bottom row displays results for sample restricted to 0-5 km vicinity of Kutapalong Expansion Site, with all gridcells ≥ 5 km south of the Expansion Site extent omitted. The two rows represent the results of two separate heterogeneity analyses. In both cases, areas > 5 km and ≤ 20 km from nearest camp boundary are omitted. Analyses each use propensity score matching to match 1km treatment and control gridcells based on pre-treatment and time-invariant observations. 30m observations within the matched 1km gridcells are used in the respective event study estimation. Standard errors clustered by 1km cluster grid.

As in the primary specification, forest loss peaks in 2019 and then declines, falling to 2.1 p.p. by 2023.

Likewise, the settlement cover event study follows a similar pattern to the primary specification, but exhibits a larger magnitude. Near Kutapalong, settlement cover increases by 4.6-4.8 p.p. by 2022-2023, substantially larger than the 3.4-3.7 p.p. increases measured in the estimations that included all camp areas.

Figure 7: Event study results for forest and settlement cover by robustness check



Notes: Estimates of Equation 1, with 2017 as the reference year and 2016 coefficient representing the pre-treatment trend. Observations are 30m grid-cells. Outcome variable is the probability of a given land cover class on the grid cell and is derived using mean composite from Dynamic World February layers for each year. Top row uses the Chittagong district as the comparison area and the 0-5 km area outside camps as the treatment area. The middle row uses gridcells 0-10 km from camp boundaries as the treatment group. The bottom row omits all grid-cells located in the Naikhongchari subdistrict, which is in Banderban district. Analyses each use propensity score matching to match 1km treatment and control gridcells based on pre-treatment and time-invariant observations. 30m observations within the matched 1km gridcells are used in the respective event study estimation. Standard errors clustered by 1km cluster grid.

6.2 Robustness checks

I combine the forest and settlement cover results for all three robustness checks in [Figure 7](#). When treatment is defined using a 0–10 km distance buffer, the matching procedure improves covariate balance considerably, with absolute standardized mean differences minimized across all matched variables ([Figure A12](#)). Results for forest cover closely align with those from the primary specification, though the estimated effects are slightly smaller in magnitude. For instance, forest loss in 2019 within the 0–10 km treatment area is 3.6 percentage points, compared to 4.6 percentage points in the main specification. This suggests that forest cover impacts were somewhat more concentrated near the camp boundary. In contrast, the settlement cover results for the 0–10 km sample are nearly identical to those in the primary analysis, indicating that the economic agglomeration effects likely extend beyond the 5 km periphery.

Next, I examine results using a comparison sample drawn from across the Chittagong district, located directly north of Cox’s Bazar. The matching procedure substantially reduces propensity score differences, though mean differences remain sizable for some covariates ([Figure A14](#)). In particular, matched treatment and control means differ more within years for settlement cover ([Table A6](#)). Mapping the matched 1 km grids shows that the Chittagong comparison sample is distributed widely across the district ([Figure A15](#)). Although this matching specification produces somewhat weaker covariate balance than other estimations, the results continue to support the primary findings. Forest cover losses again peak in 2019 before abating, with losses of about 5 percentage points in 2019 declining to zero by 2023. Settlement cover expansion appears more gradual under this specification, possibly reflecting weaker covariate balance for that variable. Even so, the event study indicates significant and steadily increasing settlement growth from 2020 onward, rising from 1.2 percentage points in 2020 to 3.2 percentage points in 2023.

Finally, I remove observations from the Naikhongchari subdistrict (Bandarban District) and repeat the analysis. The matching procedure substantially reduces mean differences across all covariates ([Figure A16](#)), yielding a highly balanced panel ([Table A7](#)). The resulting event study estimates closely mirror those of the primary specification in

both sign and magnitude, as well as in their dynamic trends. The only notable difference is a weakly significant pre-treatment trend for forest cover, though the coefficient is very small in magnitude. Overall, these findings indicate that including Naikhongchari in the main sample does not substantially affect the primary results.

6.3 Mediation analysis

The primary results, as well as a series of robustness checks, demonstrate a shift in trends, from forest decline to forest recovery, that occurs between February 2019 and February 2020. This aligns with the timing of the LPG cookstove rollouts, which reached over 100,000 households by late 2019 (see [Section 3.4](#)) and had a clear impact on energy consumption ([Figure 3](#)). My analysis thus offers suggestive evidence that the clean technology program may have abated forest losses in the camp hosting region. But the stove roll-out also coincides with fencing construction which, independent of the stoves, may have greatly augmented the cost of accessing natural areas for foraging.

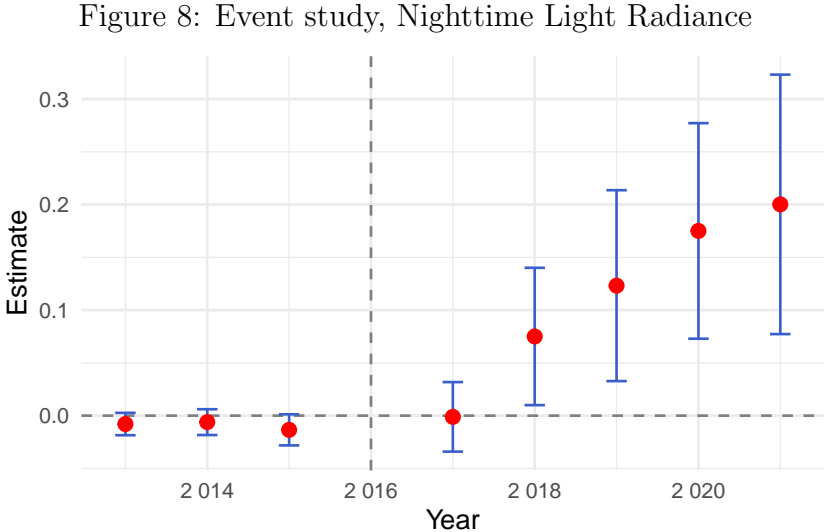
In either case, the alignment of these interventions with the shift in forest loss trends suggests that refugee biofuel harvesting had a local, direct, and negative effect on nearby forest cover. This effect, in turn, subsides once demand for biofuels falls and the cost of harvesting rises. Determining which of the two interventions drove the abatement is beyond the scope of the current study, as this requires high-frequency, high-resolution data on both stove rollouts and fencing construction.

The settlement expansion, however, points to the general equilibrium effect of camps. Increased demand from population growth, further boosted through large and regular inflows of foreign aid, may augment economic activity. To explore this further, I estimate the specification using a panel of 500 m grid-cells and VIIRS Version 2.1 Nighttime Lights masked mean radiance data from 2013 to 2021. The matching procedure substantially reduces differences in propensity scores, although standardized mean differences remain greater than 0.1 for several pre-treatment years ([Figure A18](#)). Average radiance levels, measured over relatively large 500 m grid-cells in rural areas, are very low ([Table A8](#)); for instance, on a scale with a maximum of 63, the mean radiance in the matched treatment area in 2016—the year prior to treatment—is only 0.05. The low overall radiance and

limited spatial variation influence the matching procedure, as illustrated in Figure A19. Once the highest-propensity grid-cells are matched, subsequent matches are determined primarily by ordering, producing sharp geographic clustering patterns.

Using this matched sample and clustering based on gridcell intersections with a 2km grid, my event study results suggest that camp opening drives dramatic increases in nighttime light radiance over time. Like the settlement expansion, the trend increases over the time series. By 2021, the increase in radiance reaches 0.2, representing a quadrupling of baseline levels.

This expansion in nighttime lights supports the theory of settlement land cover expansion in response to increased economic production. My analysis suggests that forest cover is indeed recovering in the camp vicinities. But settlement expansion due to local economic growth is also taking place. The results for settlement and nighttime lights provide strong evidence of the indirect effects hypothesis: that the general equilibrium effect also has implications for the landscape that can come at the expense of natural areas.



Notes: Estimates of Equation 1, with 2016 as the reference year and 2013–2015 representing pre-treatment years. Observations are 500 m grid-cells in Cox’s Bazar district or Naikhongchari subdistrict. The outcome is mean nighttime lights radiance (VIIRS Annual Composite V2.1). Treatment areas are 0–5 km from the nearest camp boundary. Areas > 5 km and ≤ 20 km are omitted. Propensity score matching conducted using the 500m grid-cells. Standard errors clustered based on intersections with 2km grid.

7 Conclusion

This paper examines the impact of high-density, large-population refugee camps on land cover. I focus on the refugee camp areas of Cox Bazar and how land cover changed in response to the large influx of Rohingya refugees starting in August 2017.

I use the high-resolution (10m) Dynamic World land cover dataset (2016-2023) to generate February mean composites of the probability a 30m grid-cell has forest, vegetation, settlement, or agricultural cover for each year. I apply a matched difference-in-differences event study approach to examine the effect on land cover in the local area 0-5km from the nearest camp boundary. To explore heterogeneous effects, I repeat my analysis for grid-cells in protected areas and exclusively for the region near the Kutapalong Expansion Site. I evaluate the robustness of my results by performing my analysis with an alternative treatment area (0-10 km), using the Chittagong district to generate a matched comparison sample, and omitting the Naikhongchari subdistrict from my dataset.

My primary results demonstrate an immediate and significant decline in forest cover during the first two years of camp opening, which reached 4.6 p.p. in 2019. Losses in 2019 are also significant and large in protected areas (3.2 p.p.) and are especially acute when restricting to the Kutapalong Expansion Site (5.8 p.p.). But across all specifications, forest losses abate after 2019 and are relatively small relative to baseline by the end of the study period (1.7 p.p. in 2023 for the primary specification). This shift in trends likely reflects one of two coinciding interventions: the large-scale rollout of LPG stoves for refugees and some local hosts, and the enclosure of camp areas in fencing, meant to contain the refugee population.

Settlement expansions intensify throughout the study period, amounting to a 3.4-3.7 p.p. increase as of 2022-2023. These settlement expansions are more pronounced in the Kutapalong Expansion Site vicinity (4.6-4.8 p.p. in 2022-2023). Mediation analysis demonstrates a monotonic increase in nighttime lights mean radiance 2017-2021, which suggests an increase in economic production over the time series. This production expansion results in more settlement as Bangladeshis move closer to the camp areas and establish brick-and-mortar businesses. Nighttime lights may also reflect public invest-

ment, and settlement expansion could be due to an increase in public works (ex: water treatment facilities) in response to a growing population and increased access to aid resources.

My results are robust to a suite of tests. In particular, a change in the treatment area from 0-5 km to 0-10 km results in marginally lower forest losses, suggesting that deforestation impacts are more intense near camp boundaries. By contrast, settlement expansion results remain the same, which aligns with past research indicating an economic agglomeration effect of up to 10 km from camp boundaries.

The findings speak to both the local direct (biofuel harvesting) and indirect (migration, economic production) effects of camp hosting on the landscape. While targeted policy may ameliorate the former, landscape transformation due to settlement expansion and economic growth will crowd out natural capital. The latter result suggests that some forest losses in the area may be permanent.

I recommend that future work further explore the direct effect to isolate which of the two interventions drive the deforestation abatement. UNHCR's pro-bono LPG program is expensive to maintain, and if research can clearly show that it is causing these forest cover improvements, I believe this would help motivate its continued funding.

On the other hand, if the observed forest recovery is primarily a consequence of the fencing and enclosure of refugee camps, further attention must be given to identifying more ethical and sustainable alternatives. Restricting refugee mobility violates Article 26 of the 1951 Refugee Convention, which guarantees the right to freedom of movement, and contradicts UNHCR guidelines discouraging the detention of refugees and asylum seekers. If fencing has indeed contributed to reduced deforestation, policymakers should critically reassess this approach and instead pursue strategies that protect both natural capital and human rights in Cox's Bazar.

References

- Abadie, A., S. Athey, G. W. Imbens, and J. M. Wooldridge (2023). When should you adjust standard errors for clustering? *The Quarterly Journal of Economics* 138(1), 1–35.
- Alix-Garcia, J. and D. L. Millimet (2023). Remotely incorrect? accounting for nonclassical measurement error in satellite data on deforestation. *Journal of the Association of Environmental and Resource Economists* 10(5), 1335–1367.
- Alix-Garcia, J. and D. Saah (2010). The effect of refugee inflows on host communities: Evidence from Tanzania. *The World Bank Economic Review* 24(1), 148–170.
- Alix-Garcia, J., S. Walker, A. Bartlett, H. Onder, and A. Sanghi (2018). Do refugee camps help or hurt hosts? the case of Kakuma, Kenya. *Journal of Development Economics* 130, 66–83.
- Amnesty International (2016a). Bangladesh pushes back Rohingya refugees amid collective punishment in Myanmar. Amnesty International. <https://www.amnesty.org/en/latest/press-release/2016/11/bangladesh-pushes-back-rohingya-refugees-amid-collective-punishment-in-myanmar/>.
- Amnesty International (2016b). Myanmar: Security forces target Rohingya during vicious rakhine scorched-earth campaign. Amnesty International. <https://www.amnesty.org/en/latest/press-release/2016/12/myanmar-security-forces-target-rohingya-viscious-scorched-earth-campaign/>.
- Aung, B. M., Y. Sumarlan, M. G. Hayes, and S. M. A. Rahman (2015). *An Examination on the Situation of Undocumented Muslim Refugees from Rakhine State: A Case Study of Two Refugee Camps in Bangladesh*. Mahidol University.
- Baird, S., A. C. Davis, M. Genoni, P. Lopez-Pena, A. M. Mobarak, N. Palaniswamy, J. Seager, and T. Vishwanath (2021). Cox’s Bazar Panel Survey, 2019 (Bangladesh). Technical report, World Bank.
- Bangladesh Bureau of Statistics (2014). Population housing census 2011: National report volume ii. Technical report, Ministry of Planning.
- Bangladesh Bureau of Statistics (2022). Population and housing census 2022: Preliminary report. Technical report, Ministry of Planning.
- Bangladesh Bureau of Statistics (2023). Population and housing census 2022: National report volume i. Technical report, Ministry of Planning.
- BenarNews (2017). Rohingya influx brings ‘environmental catastrophe’: Bangladesh officials. Radio Free Asia. <https://www.rfa.org/english/news/myanmar/refugees-environment-10302017171539.html>.
- Bertrand, M., E. Duflo, and S. Mullainathan (2004). How much should we trust differences-in-differences estimates? *The Quarterly journal of economics* 119(1), 249–275.
- Betts, A., L. Bloom, J. D. Kaplan, and N. Omata (2017). *Refugee economies: Forced displacement and development*. Oxford University Press.

- Black, R. (1998). *Refugees, Environment and Development*. Routledge.
- Black, R. and M. Sessay (1999). Forced migration, natural resource use and environmental change: The case of the Senegal river valley. *International Journal of Population Geography*, 4(1)..
- Blakemore, E. (2019). The Rohingya people: Facts and information.
- Blinken, A. (2022). United States and allies impose additional sanctions on the Burmese military regime.
- Brown, C. F., S. P. Brumby, B. Guzder-Williams, A. M. Tait, et al. (2022). Dynamic World: Near real-time global 10 m land use/land cover mapping. *Scientific Data* 9, 251.
- Bruederle, A. and R. Hodler (2018). Nighttime lights as a proxy for human development at the local level. *PloS One* 13(9).
- Cameron, A. C. and D. L. Miller (2015). A practitioner’s guide to cluster-robust inference. *Journal of Human Resources* 50(2), 317–372.
- Chittagong Hill Tracts Commission (2000). ‘Life is not ours’: Land and human rights in the Chittagong Hill Tracts, Bangladesh. Technical report, Chittagong Hill Tracts Commission.
- Dampha, N. K., C. Salemi, and S. Polasky (2022). Rohingya refugee camps and forest loss in Cox’s Bazar, Bangladesh: An inquiry using remote sensing and econometric approaches. Technical report, The World Bank.
- d’Errico, M., R. D. Mariani, R. Pietrelli, and F. C. Rosati (2022). Refugee-host proximity and market creation in Uganda. *The Journal of Development Studies* 58(2), 213–233.
- Farzana, K. F. (2017). *Memories of Burmese Rohingya refugees: Contested identity and belonging*. Springer.
- Filipski, M. J., G. Rosenbach, E. Tiburcio, P. Dorosh, and J. Hoddinott (2021). Refugees who mean business: economic activities in and around the Rohingya settlements the Rohingya settlements in Bangladesh. *Journal of Refugee Studies* 34(1), 1202–1242.
- Fortify Rights (2020). Bangladesh: Remove fencing that confines Rohingya to refugee camps. <https://www.fortifyrights.org/bgd-inv-2020-10-09-2/>.
- Hasan, M. E., L. Zhang, R. Mahmood, H. Guo, and G. Li (2021). Modeling of forest ecosystem degradation due to anthropogenic stress: the case of Rohingya influx into the Cox’s Bazar-Teknaf Peninsula of Bangladesh. *Environments* 8(11).
- Health Sector Coordination Team (2021, December). Bangladesh: Emergency—Rohingya refugee/FDMN crisis in Cox’s Bazar district, health sector bulletin #17. Technical report, World Health Organization (WHO) and Health Sector Partners, Cox’s Bazar, Bangladesh. Reporting period: October–December 2021.
- Heckman, J. J., H. Ichimura, and P. E. Todd (1997). Matching as an econometric evaluation estimator: Evidence from evaluating a job training programme. *The Review of Economic Studies* 64(4), 605–654.

- Human Rights Council (2022). Report of the independent investigative mechanism for Myanmar: Fifty-first session, agenda item 4. Technical report, United Nations General Assembly.
- Human Rights Watch (2000). Burmese refugees in bangladesh: Still no durable solution. Technical report, Refworld, C1203.
- Ibrahim, A. (2016). *The Rohingyas: Inside Myanmar's hidden genocide*. Hurst Company.
- International, A. (2017). Myanmar: Crimes against humanity terrorize and drive Rohingya out. Amnesty International. <https://www.amnesty.org/en/latest/news/2017/10/myanmar-new-evidence-of-systematic-campaign-to-terrorize-and-drive-rohingya-out/>.
- ISCG (2018). Bangladesh—outline of camps of Rohingya refugees in Cox's Bazar. <https://data.humdata.org/dataset/outline-of-camps-sites-of-Rohingya-refugees-in-cox-s-bazar-bangladesh>.
- IWGIA, Organising Committee CHT Campaign, and Shimin Gaikou Centre (2012). Militarization in the Chittagong Hill Tracts, Bangladesh: The slow demise of the region's indigenous peoples. Technical report, IWGIA and Organising Committee CHT Campaign and Shimin Gaikou Centre.
- Jacobsen, K. (1994). Impact of refugees on the environment: A review of the evidence. Technical report, Refugee Policy Group, Washington, DC.
- Jakes, L. (2022). Myanmar's military committed genocide against Rohingya, u.s. says—the new york times. <https://www.nytimes.com/2022/03/21/us/politics/myanmar-genocide-biden.html>.
- Kibreab, G. (1997). Environmental causes and impact of refugee movements: A critique of the current debate. *Disasters*, 21(1), 20–38..
- Martinez, L. R. (2022). How much should we trust the dictator's GDP growth estimates? *Journal of Political Economy* 130(10).
- Maystadt, J.-F., V. Mueller, J. Van Den Hoek, and S. Van Weezel (2020). Vegetation changes attributable to refugees in africa coincide with agricultural deforestation. *Environmental Research Letters* 15(4), 044008.
- Maystadt, J.-F. and P. Verwimp (2014). Winners and losers among a refugee-hosting population. *Economic Development and Cultural Change* 62(4), 769–809.
- Mohshin Habib, C. (2018). Forced migration of Rohingya: The untold experience.
- Nebehay, S. (2017). U.N. sees “textbook example of ethnic cleansing” in Myanmar — Reuters.
- Parnini, S. N., M. R. Othman, and A. S. Ghazali (2013). The Rohingya refugee crisis and Bangladesh-Myanmar relations. *Asian and Pacific Migration Journal* 22(1), 133–146.
- Rahman, M., M. Islam, and T. Chowdhury (2018). Change of vegetation cover at Rohingya refugee occupied areas in Cox's Bazar district of Bangladesh: evidence from remotely sensed data. *Journal of Environmental Science and Natural Resources* 11(1-2), 9–16.

- Reuters (2017). At least 71 killed in Myanmar as Rohingya insurgents stage major attack.
- Roth, J., P. H. Sant'Anna, A. Bilinski, and J. Poe (2023). What's trending in difference-in-differences? a synthesis of the recent econometrics literature. *Journal of Econometrics* 235(2), 2218–2244.
- Rozo, S., M. Urbina, A. Etang Ndip, and C. Wieser (2024). Refugees and humanitarian aid: The Rohingya impact on Bangladesh's development. *Available at SSRN 4972680*.
- Salemi, C. (2021). Refugee camps and deforestation in Sub-Saharan Africa. *Journal of Development Economics* 152, 102682.
- Sarkar, S. K., M. Saroar, and T. Chakraborty (2023). Navigating nature's toll: Assessing the ecological impact of the refugee crisis in Cox's Bazar, Bangladesh. *Heliyon* 9(7).
- Smith, J. A. and P. E. Todd (2001). Reconciling conflicting evidence on the performance of propensity-score matching methods. *American Economic Review* 91(2), 112–118.
- Tan, V. (2017). Give the Rohingya hope for a future, urges UNHCR chief.
- Tay, A. K., R. Islam, A. Riley, C. Welton-Mitchell, B. Duchesne, V. Waters, A. Varner, D. Silove, and P. Ventevogel (2018). Culture, context, and mental health of Rohingya refugees: A review for staff in mental health and psychosocial support programmes for Rohingya refugees. Technical report, UNHCR.
- Taylor, J. E., M. J. Filipowski, M. Alloush, A. Gupta, R. I. Rojas Valdes, and E. Gonzalez-Estrada (2016). Economic impact of refugees. *Proceedings of the National Academy of Sciences* 113(27), 7449–7453.
- Ullah, A. A. (2011). Rohingya refugees to Bangladesh: Historical exclusions and contemporary marginalization. *Journal of Immigrant & Refugee Studies* 9(2).
- UNEP-WCMC and IUCN (2021). Protected Planet: The world database on protected areas (WDPA) and world database on other effective area-based conservation measures (wd-oecm).
- UNHCR (2007). Bangladesh: Analysis of gaps in the protection of Rohingya refugees. Technical report, UNHCR.
- UNHCR (2017a). UNHCR operational update: Bangladesh, 17 november 2017. Technical report, UNHCR.
- UNHCR (2017b). UNHCR operational update: Bangladesh, 20 october 2017. Technical report, UNHCR.
- UNHCR (2017c). UNHCR operational update: Bangladesh, 3 november 2017. Technical report, UNHCR.
- UNHCR (2017d). UNHCR operational update: Bangladesh, 6 october 2017. Technical report, UNHCR.
- UNHCR (2018a). UNHCR operational update: Bangladesh, 16-22 january 2018. Technical report, UNHCR.

- UNHCR (2018b). UNHCR operational update: Bangladesh, 5-20 june 2018. Technical report, UNHCR.
- UNHCR (2018c). UNHCR operational update: Bangladesh, 9 may—4 june 2018. Technical report, UNHCR.
- UNHCR (2019). Rohingya refugee response, Bangladesh: Refugee population density (as of 15 august 2019).
- UNHCR (2020). UNHCR operational update, external, july 2020. Technical report, UNHCR.
- UNHCR (2022). Refugee Environmental Protection Fund. <https://www.unhcr.org/what-we-do/how-we-work/environment-disasters-and-climate-change/refugee-environmental-protection>.
- UNHCR and WFP (2021). Jam Cox’s Bazar 2021: UNHCR-WFP joint assessment mission report, Cox’s Bazar, Bangladesh, july 2021. Technical report, UNHCR.
- Venter, Z. S., D. N. Barton, T. Chakraborty, T. Simensen, and G. Singh (2022). Global 10 m land use land cover datasets: A comparison of Dynamic World, World Cover and Esri Land Cover. *Remote Sensing* 14(16), 4101.

Rohingya refugee camps and land cover change in Bangladesh: Technical Appendix

Colette Salemi

November 11, 2025

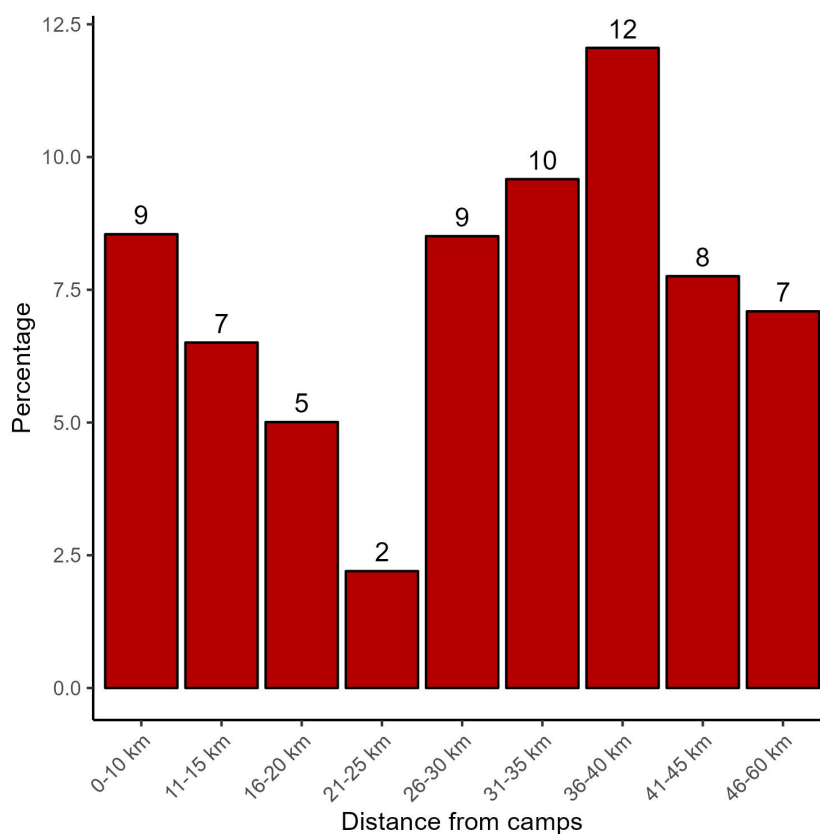
A Additional descriptive tables and figures

Table A1: Distribution of Rohingya refugee population by residence location, CBPS 2019

Residence location	Percent of Rohingya population
Camp	98.38
0-10 km from camp	0.85
11-15 km from camp	0.20
16-20 km from camp	0.25
31-35 km from camp	0.25
36-40 km from camp	0.04
46-60 km from camp	0.04
Total	100.00

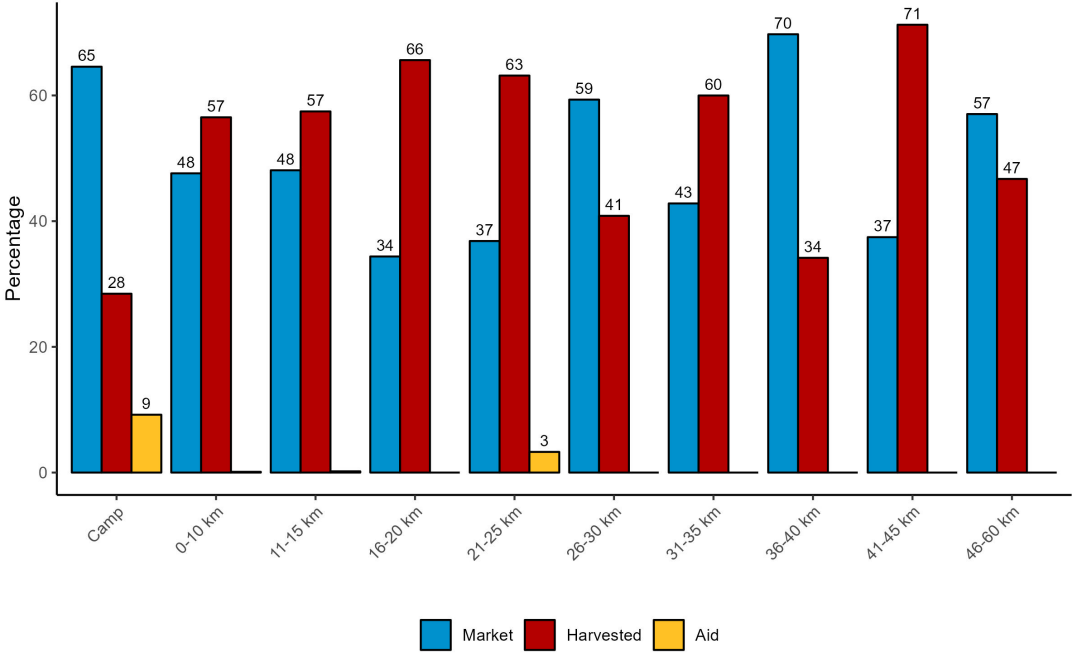
Notes: Weighted averages (using individual weights) of the share of all Rohingya individuals (including children and the elderly) residing in a camp or one of six distance-to-camp regions, compiled by the study team using Cox Bazar Panel Survey 2019 data. Distance to the nearest camp is based on non-linear travel distance, not Euclidean distance.

Figure A1: Percent of Bengali adults who arrived at place of residence after August 2017 by distance to nearest camp, CBPS 2019, CBPS 2019



Notes: Weighted averages (using individual weight) of the share of adult respondents (age 15 or older) compiled by study team using Cox Bazar Panel Survey 2019 data. Distance to nearest camp is based on non-linear travel distance, not Euclidean distance.

Figure A2: Distribution source of firewood consumption in previous week by distance to the nearest camp



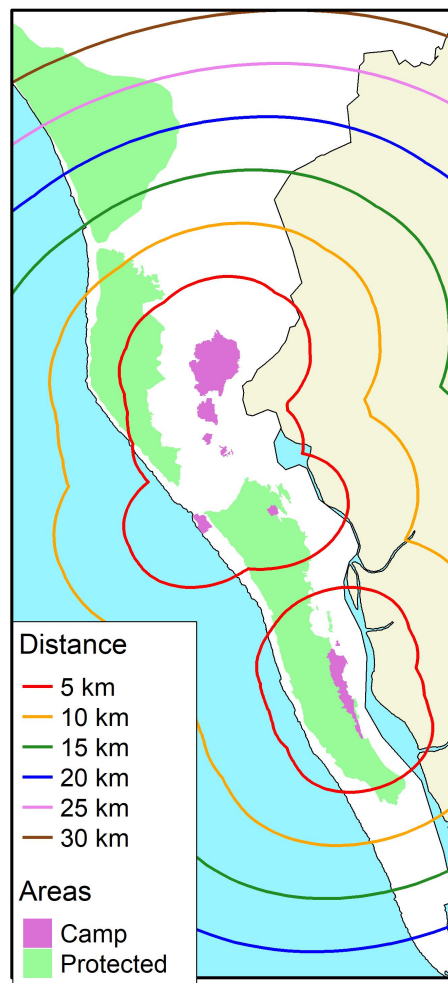
Notes: Weighted averages (using individual weight) of the share of adult respondents (age 15 or older) compiled by study team using Cox Bazar Panel Survey 2019 data. Distance to nearest camp is based on non-linear travel distance, not Euclidean distance.

Figure A3: Administrative boundaries of study area



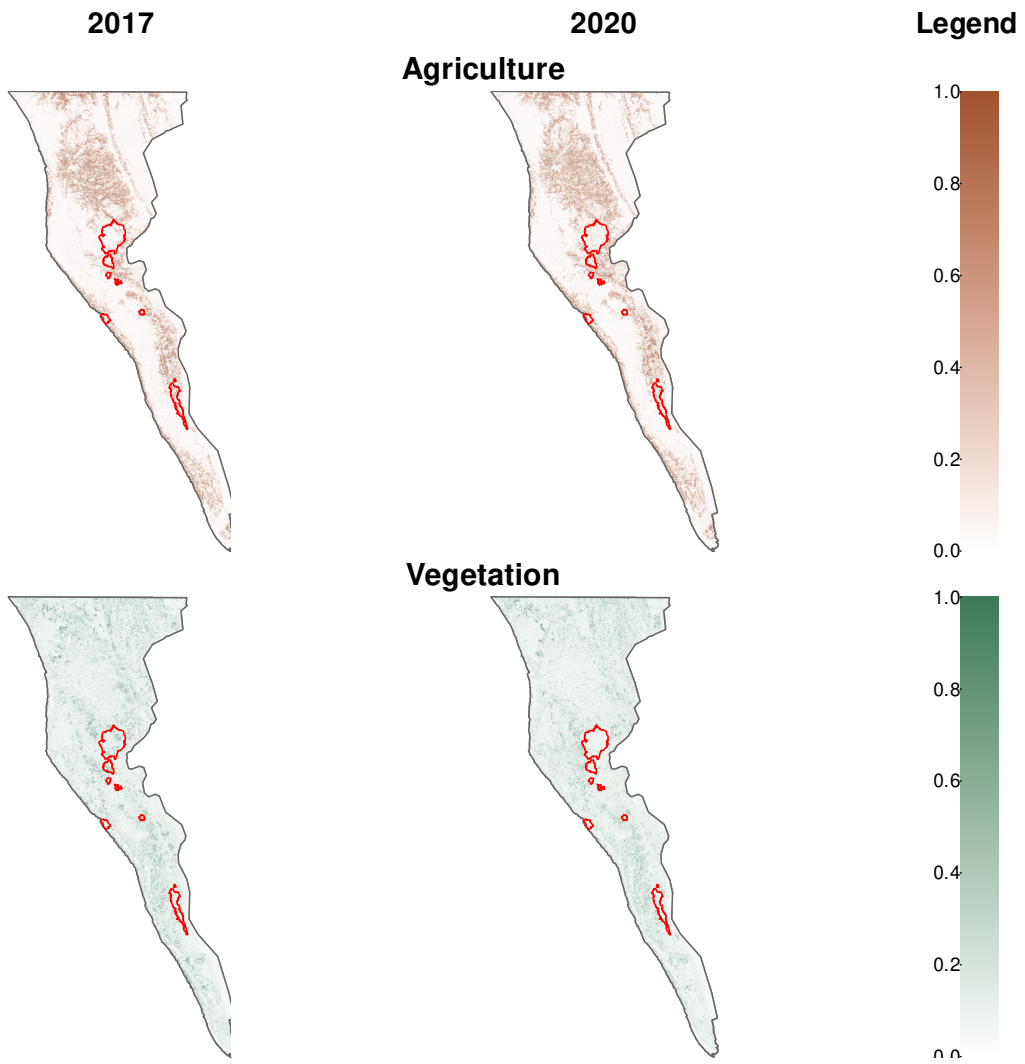
Notes: Maps produced by study team using publicly available data on administrative divisions

Figure A4: Map showing study area and distance cutoffs used for treatment assignment



Notes: Maps produced by study team using publicly available data on administrative divisions, ISWG polygon data on camp locations, and Protected Planet polygons on protected areas. Buffer lines show distances in kilometers (km) from the nearest camp boundary. I used these km cutoffs to create distance categories. In the primary analysis, the 0-5 km distance category provides the treatment group, while areas at distance $\in (5km, 20km]$ are excluded from the sample to avoid control group misclassification.

Figure A5: Probability of agriculture and vegetation cover by year in and near camps

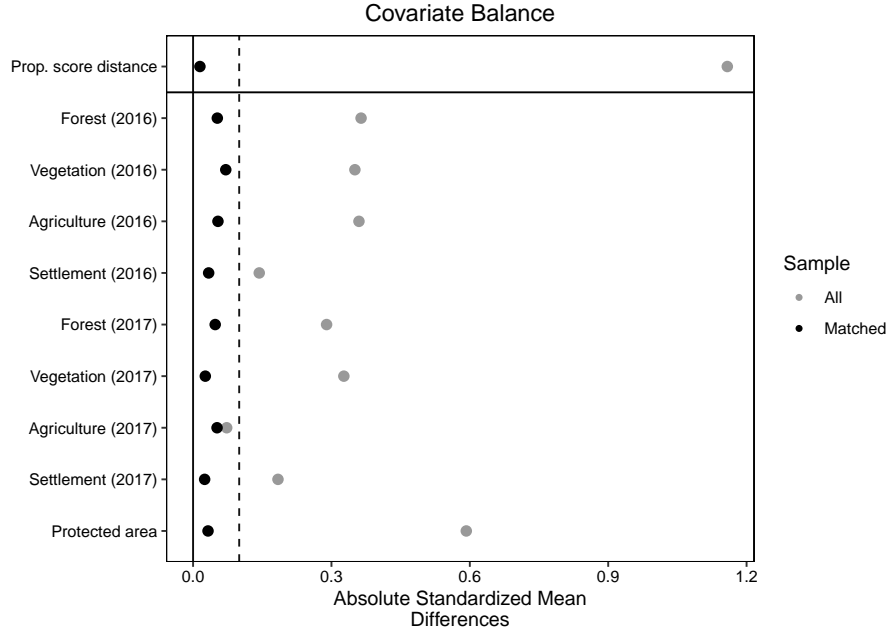


Notes: Author's production using Dynamic World probability of land cover data and are derived using mean composite from February layers for each year. Camp boundaries sourced from UNHCR and IOM Inter-Sector Working Group.

B Matching performance

B.1 Primary specification

Figure A6: Covariate balancing table from propensity score matching, primary specification



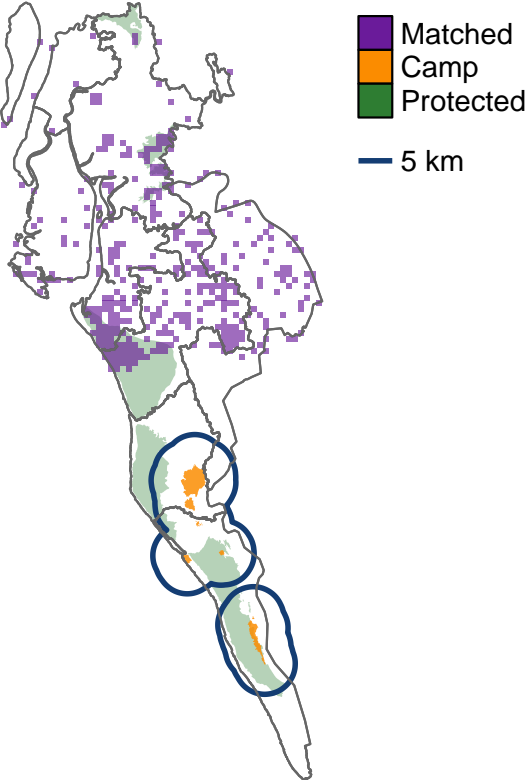
Notes: Mean probability of different land cover classes based on Dynamic World annual mean composites from February imagery for a given year and upscaled to 30m resolution. Analysis uses data from Cox Bazar district and Nakihongchari subdistrict. Treatment group is 0-5 km from a camp boundary, and control group is > 20 km from nearest camp. Absolute standardized mean differences based on nearest neighbor ($K = 1$) propensity score matching.

Table A2: Balance tests for pre-treatment years, Primary specification

Variable	Year	Control	Treated	Difference	t-stat
Settlement	2016	0.062	0.057	0.005***	30.39
	2017	0.083	0.077	0.006***	22.86
Forest	2016	0.367	0.385	-0.018***	-28.39
	2017	0.362	0.384	-0.021***	-31.98
Vegetation	2016	0.148	0.145	0.004***	16.98
	2017	0.148	0.144	0.004***	17.10
Agriculture	2016	0.148	0.139	0.009***	23.73
	2017	0.141	0.132	0.009***	26.03
Protected	2016	0.221	0.229	-0.008***	-7.93
	2017	0.221	0.229	-0.008***	-7.93
N		347,561	305,213		

Notes: Mean probability of different land cover classes based on Dynamic World annual mean composites from February imagery for a given year and upscaled to 30m resolution. Analysis uses data from Cox Bazar district and Nakihongchari subdistrict. Treatment group is 0-5 km from a camp boundary, and control group is > 20 km from nearest camp. Final groupings based on propensity score matching. Stars denote significance levels: * $p < 0.05$, ** $p < 0.01$, *** $p < 0.001$.

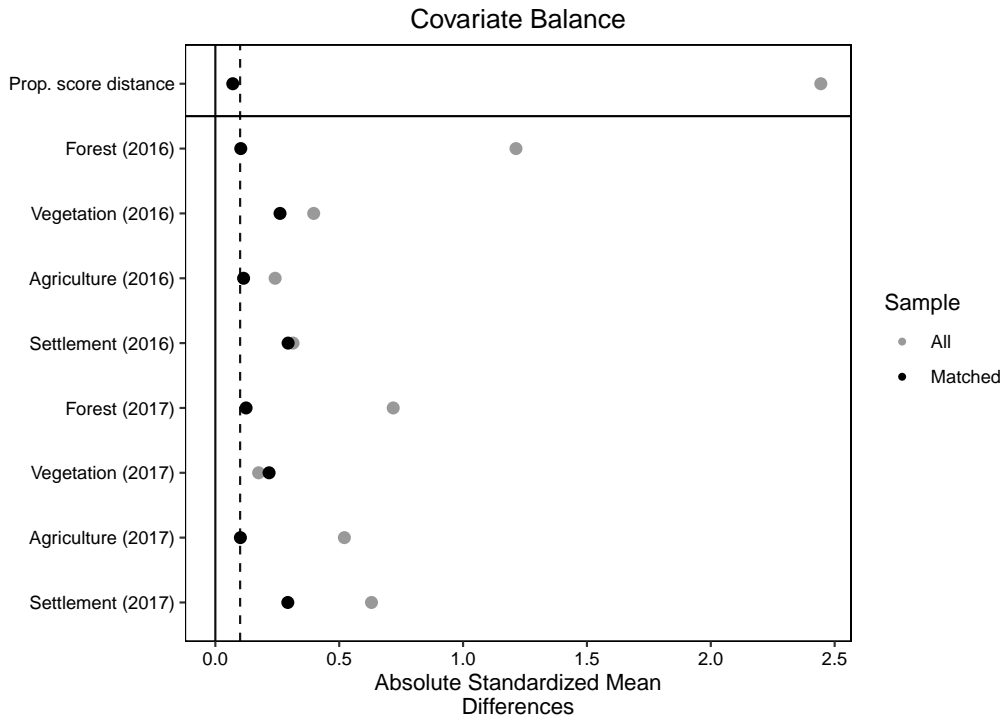
Figure A7: Control group Control group matching cluster grid locations, Primary specification



Notes: Analysis uses data from Cox Bazar district and Nakhongchari subdistrict. Treatment group is 0-5 km from a camp boundary, and control group is > 20 km from nearest camp. Final groupings based on propensity score matching. Grids represent the 1km grids used for matching and for clustering standard errors.

B.2 Protected areas only

Figure A8: Covariate balancing table from propensity score matching, Protected areas only



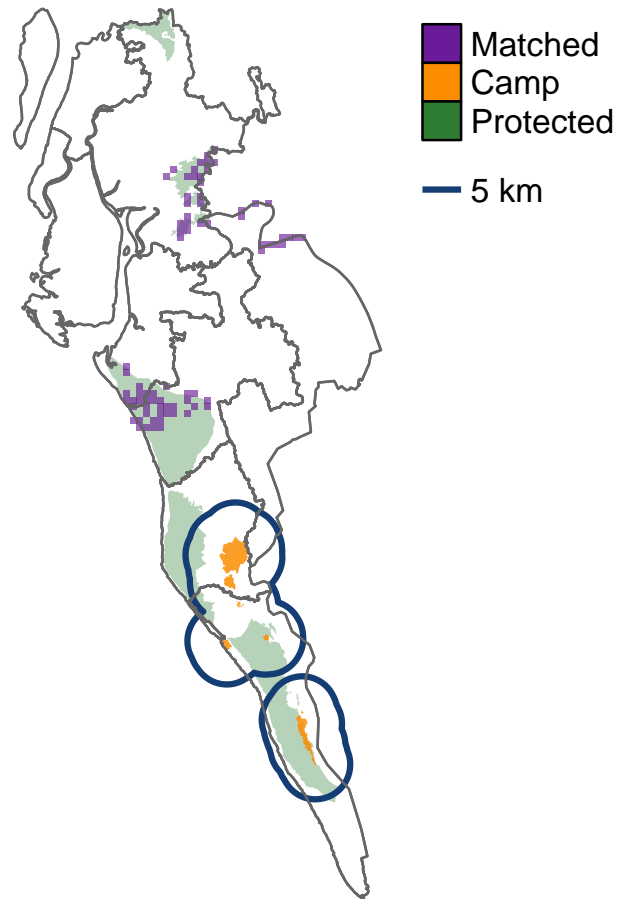
Notes: Mean probability of different land cover classes based on Dynamic World annual mean composites from February imagery for a given year and upscaled to 30m resolution. Analysis uses data from protected areas in Cox Bazar district and Nakihongchari subdistrict. Treatment group is 0-5 km from a camp boundary, and control group is > 20 km from nearest camp. Absolute standardized mean differences based on nearest neighbor ($K = 1$) propensity score matching.

Table A3: Balance tests for pre-treatment years, Protected areas only

Variable	Year	Control	Treated	Difference	t-stat
Settlement	2016	0.057	0.046	0.011***	26.06
	2017	0.074	0.056	0.019***	29.68
Forest	2016	0.468	0.548	-0.080***	-58.89
	2017	0.487	0.567	-0.080***	-54.04
Vegetation	2016	0.176	0.163	0.013***	19.88
	2017	0.161	0.146	0.015***	23.13
Agriculture	2016	0.110	0.074	0.036***	45.17
	2017	0.103	0.075	0.028***	41.18
Protected	2016	1.000	1.000	0.000	
	2017	1.000	1.000	0.000	
N		47,284	41,668		

Notes: Mean probability of different land cover classes based on Dynamic World annual mean composites from February imagery for a given year and upscaled to 30m resolution. Analysis uses data from protected areas in Cox Bazar district and Nakihongchari subdistrict. Treatment group is 0-5 km from a camp boundary, and control group is > 20 km from nearest camp. Final groupings based on propensity score matching. Stars denote significance levels: * $p < 0.05$, ** $p < 0.01$, *** $p < 0.001$.

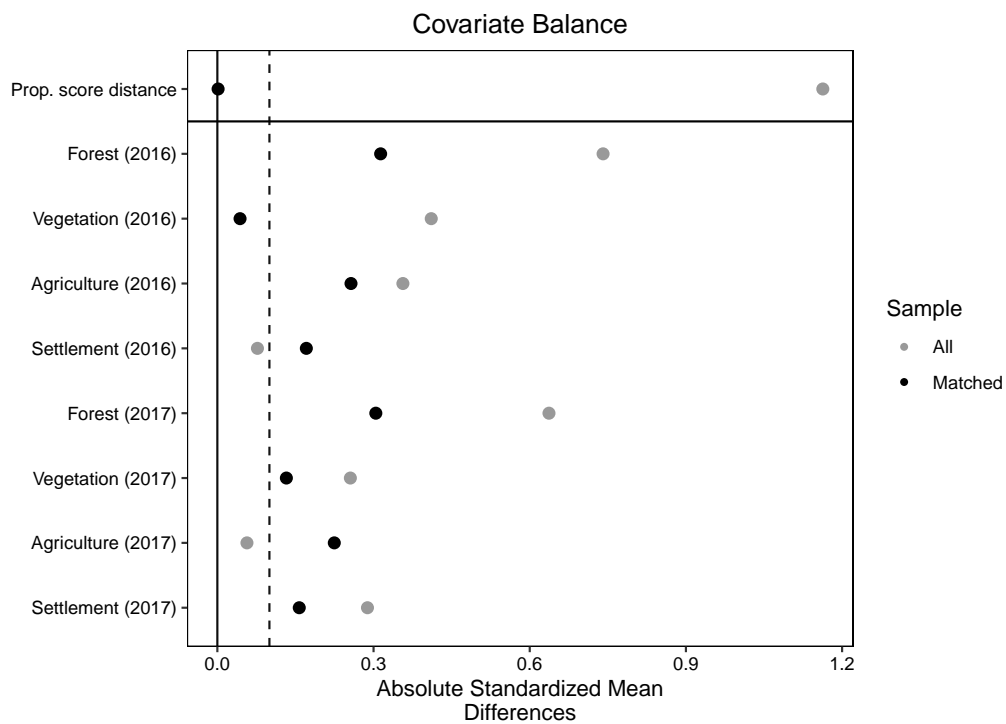
Figure A9: Control group matching cluster grid locations, protected areas only



Notes: Analysis uses data from protected areas in Cox Bazar district and Nakhongchari subdistrict. Treatment group is 0-5 km from a camp boundary, and control group is > 20 km from nearest camp. Grids represent the 1km grids used for matching and for clustering standard errors.

B.3 Kutapalong Expansion Site vicinity

Figure A10: Covariate balancing table from propensity score matching, Kutapalong Expansion Site vicinity as treatment area



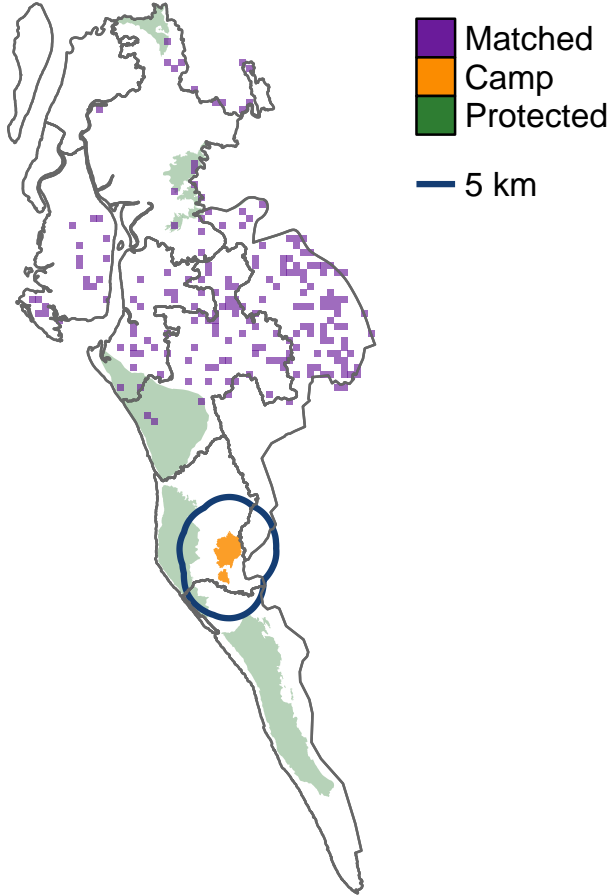
Notes: Mean probability of different land cover classes based on Dynamic World annual mean composites from February imagery for a given year and upscaled to 30m resolution. Analysis uses data from Cox Bazar district and Nakihongchari subdistrict. Treatment group is 0-5 km from Kutapalong Expansion Site boundary, and control group is > 20 km from nearest camp. Area > 5 km south of the southernmost extent of the Expansion Site or further are excluded. Absolute standardized mean differences based on nearest neighbor ($K = 1$) propensity score matching.

Table A4: Balance tests for pre-treatment years, Kutapalong Expansion Site vicinity as treatment area

Variable	Year	Control	Treated	Difference	t-stat
Settlement	2016	0.049	0.052	-0.003***	-20.06
	2017	0.064	0.072	-0.007***	-25.64
Forest	2016	0.502	0.449	0.053***	67.75
	2017	0.507	0.453	0.054***	65.71
Vegetation	2016	0.145	0.150	-0.005***	-16.94
	2017	0.137	0.144	-0.007***	-25.61
Agriculture	2016	0.111	0.133	-0.022***	-45.66
	2017	0.111	0.129	-0.018***	-40.84
Protected	2016	0.039	0.153	-0.114***	-118.12
	2017	0.039	0.153	-0.114***	-118.12
N		205,238	174,004		

Notes: Mean probability of different land cover classes based on Dynamic World annual mean composites from February imagery for a given year and upscaled to 30m resolution. Analysis uses data from Cox Bazar district and Nakihongchari subdistrict. Treatment group is 0-5 km from Kutapalong Expansion Site boundary, and control group is > 20 km from nearest camp. Area > 5 km south of the southernmost extent of the Expansion Site or further are excluded. Final groupings based on propensity score matching. Stars denote significance levels: * $p < 0.05$, ** $p < 0.01$, *** $p < 0.001$.

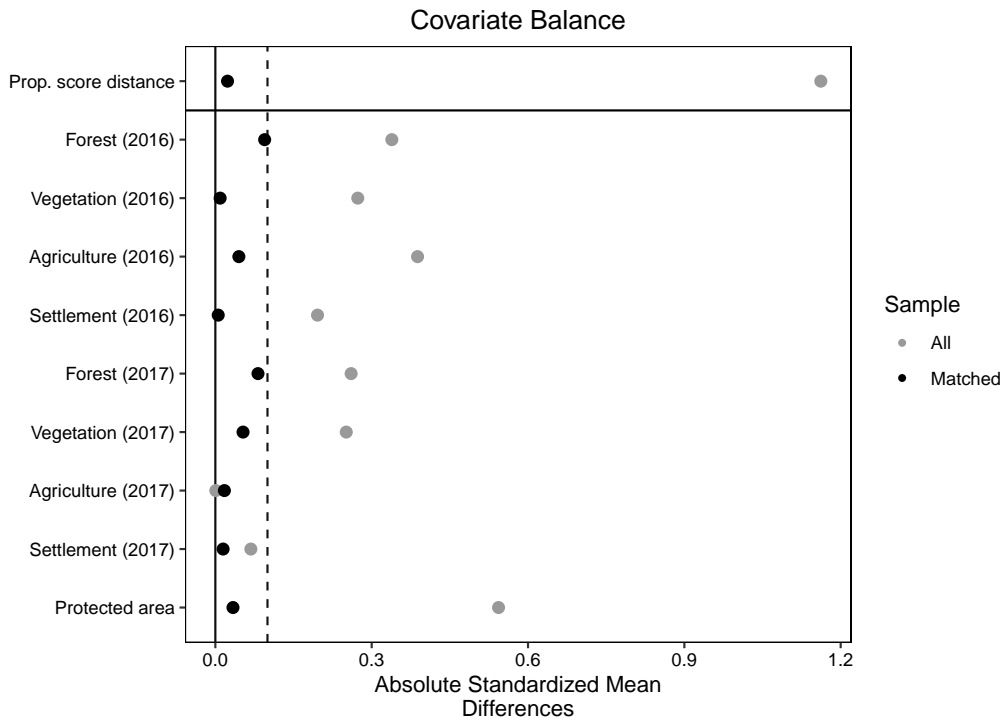
Figure A11: Control group matching cluster grid locations, Kutapalong Expansion Site vicinity as treatment area



Notes: Analysis uses data from Cox Bazar district and Nakihongchari subdistrict. Treatment group is 0-5 km from Kutapalong Expansion Site boundary, and control group is > 20 km from nearest camp. Area > 5 km south of the southernmost extent of the Expansion Site or further are excluded. Grids represent the 1km grids used for matching and for clustering standard errors.

B.4 0-10 km treatment area

Figure A12: Covariate balancing table from propensity score matching, 0-10 km treatment area



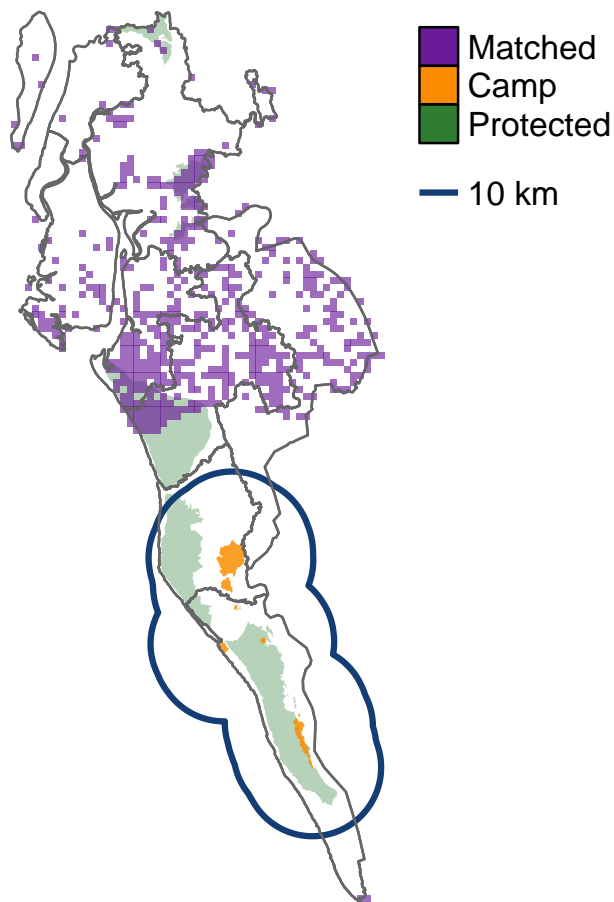
Notes: Mean probability of different land cover classes based on Dynamic World annual mean composites from February imagery for a given year and upscaled to 30m resolution. Analysis uses data from Cox Bazar district and Nakihongchari subdistrict. Treatment group is 0-10 km from a camp boundary, and control group is > 20 km from nearest camp. Absolute standardized mean differences based on nearest neighbor ($K = 1$) propensity score matching.

Table A5: Balance tests for pre-treatment years, 0-10 km treatment area

Variable	Year	Control	Treated	Difference	t-stat
Settlement	2016	0.063	0.062	0.002***	10.12
	2017	0.087	0.086	0.002***	7.65
Forest	2016	0.357	0.368	-0.011***	-21.31
	2017	0.349	0.364	-0.015***	-26.76
Vegetation	2016	0.141	0.140	0.001***	5.16
	2017	0.140	0.142	-0.002***	-9.10
Agriculture	2016	0.156	0.152	0.004***	11.02
	2017	0.155	0.147	0.008***	26.15
Protected	2016	0.172	0.195	-0.023***	-28.76
	2017	0.172	0.195	-0.023***	-28.76
N		510,308	457,243		

Notes: Mean probability of different land cover classes based on Dynamic World annual mean composites from February imagery for a given year and upscaled to 30m resolution. Analysis uses data from Cox Bazar district and Nakihongchari subdistrict. Treatment group is 0-10 km from a camp boundary, and control group is > 20 km from nearest camp. Final groupings based on propensity score matching. Stars denote significance levels: * $p < 0.05$, ** $p < 0.01$, *** $p < 0.001$.

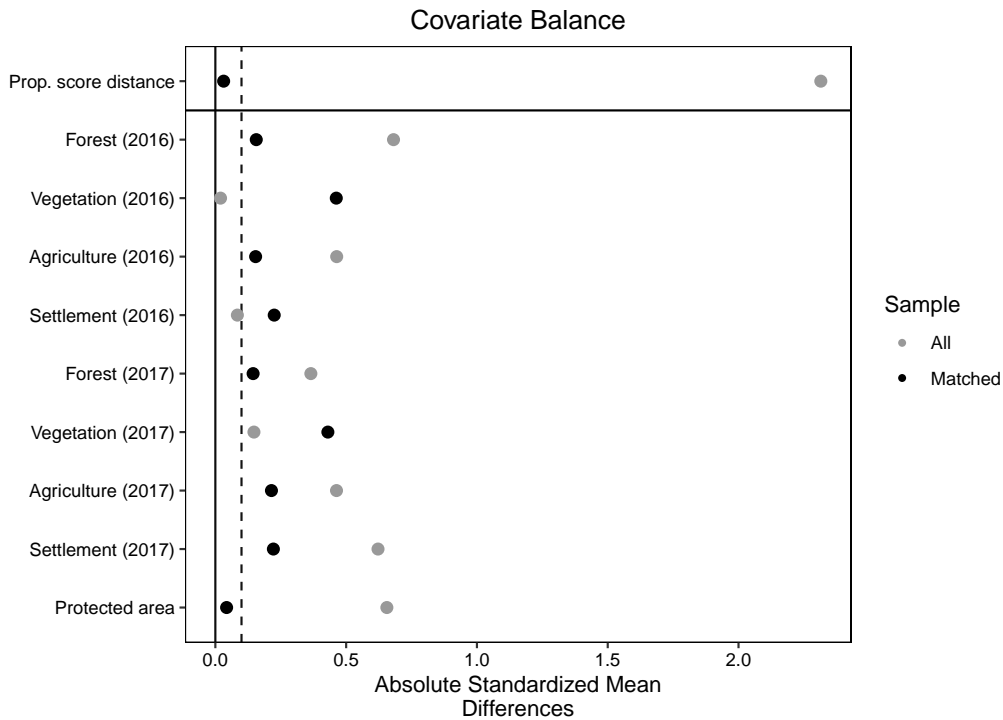
Figure A13: Control group matching cluster grid locations, 0-10 km treatment area



Notes: Analysis uses data from Cox Bazar district and Nakihongchari sub-district. Treatment group is 0-10 km from a camp boundary, and control group is > 20 km from nearest camp. Final groupings based on propensity score matching. Grids represent the 1km grids used for matching and for clustering standard errors.

B.5 Chittagong comparison sample

Figure A14: Covariate balancing table from propensity score matching, Chittagong comparison sample



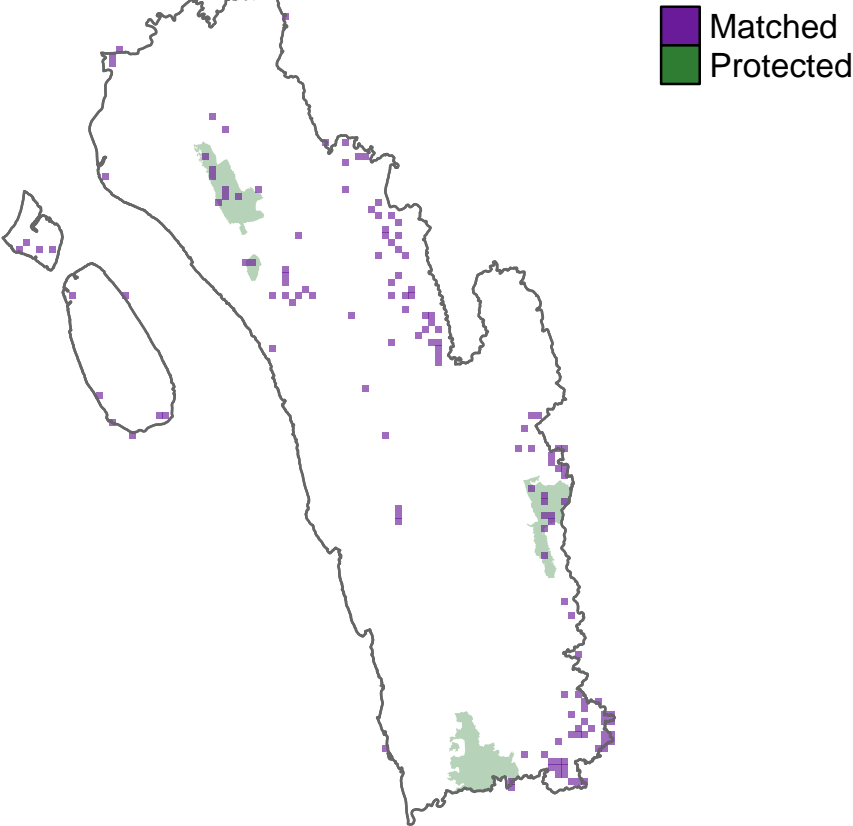
Notes: Mean probability of different land cover classes based on Dynamic World annual mean composites from February imagery for a given year and upscaled to 30m resolution. Analysis uses data from Cox Bazar district, Chittagong District, and Nakihongchari subdistrict. Treatment group is 0-5 km from a camp boundary, and control group is drawn from Chittagong district. Absolute standardized mean differences based on nearest neighbor ($K = 1$) propensity score matching.

Table A6: Balance tests for pre-treatment years, Chittagong comparison sample

Variable	Year	Control	Treated	Difference	t-stat
Settlement	2016	0.059	0.047	0.012***	52.99
	2017	0.074	0.059	0.015***	43.61
Forest	2016	0.353	0.356	-0.003**	-3.20
	2017	0.368	0.369	-0.001	-0.71
Vegetation	2016	0.164	0.140	0.024***	65.64
	2017	0.154	0.130	0.024***	65.27
Agriculture	2016	0.144	0.107	0.036***	65.85
	2017	0.153	0.112	0.041***	71.70
Protected	2016	0.136	0.118	0.019***	14.06
	2017	0.136	0.118	0.019***	14.06
N		138,173	114,754		

Notes: Mean probability of different land cover classes based on Dynamic World annual mean composites from February imagery for a given year and upscaled to 30m resolution. Analysis uses data from Cox Bazar district, Chittagong district, and Nakihongchari subdistrict. Treatment group is 0-5 km from a camp boundary, and control group is drawn from Chittagong district. Final groupings based on propensity score matching. Stars denote significance levels: * $p < 0.05$, ** $p < 0.01$, *** $p < 0.001$.

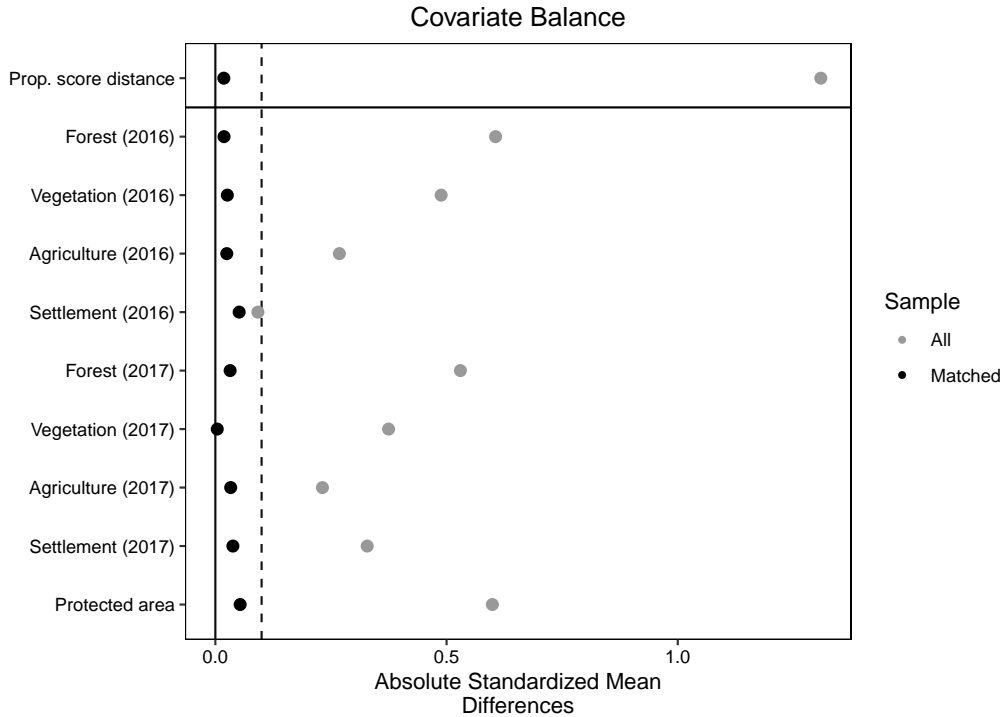
Figure A15: Control group matching cluster grid locations, Chittagong comparison sample



Notes: Analysis uses data from Cox Bazar district and Nakihongchari subdistrict. Treatment group is 0-5 km from a camp boundary, and control group is drawn from Chittagong district. Final groupings based on propensity score matching. Grids represent the 1km grids used for matching and for clustering standard errors.

B.6 Omitting Banderban

Figure A16: Covariate balancing table from propensity score matching, Banderban district omitted



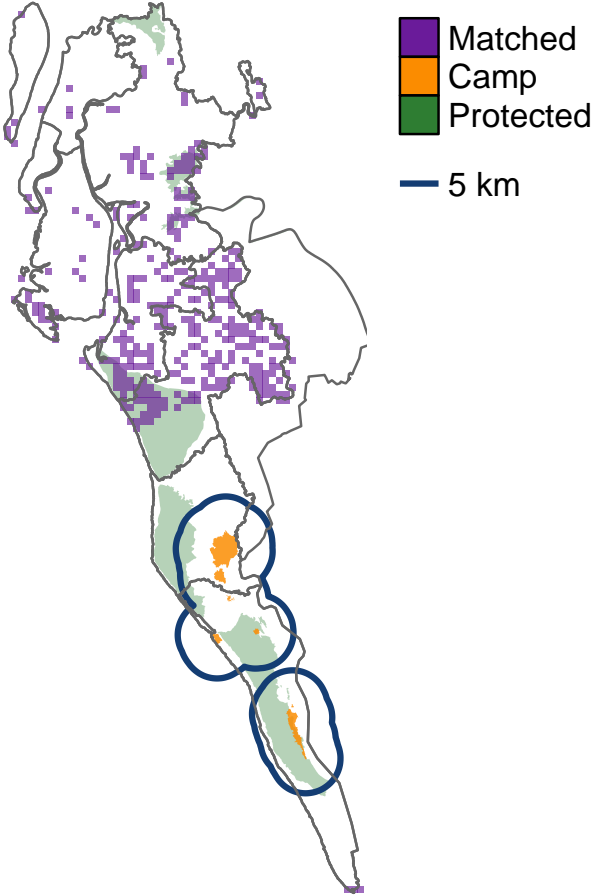
Notes: Mean probability of different land cover classes based on Dynamic World annual mean composites from February imagery for a given year and upscaled to 30m resolution. Analysis uses data from Cox Bazar district. Treatment group is 0-5 km from a camp boundary, and control group is > 20 km from nearest camp. Absolute standardized mean differences based on nearest neighbor ($K = 1$) propensity score matching.

Table A7: Balance tests for pre-treatment years, Banderban district omitted

Variable	Year	Control	Treated	Difference	t-stat
Settlement	2016	0.062	0.058	0.005***	26.18
	2017	0.083	0.078	0.005***	18.71
Forest	2016	0.345	0.376	-0.031***	-45.18
	2017	0.338	0.374	-0.036***	-51.66
Vegetation	2016	0.142	0.143	-0.001***	-4.92
	2017	0.146	0.143	0.003***	13.30
Agriculture	2016	0.160	0.141	0.019***	46.51
	2017	0.153	0.134	0.019***	50.59
Protected	2016	0.191	0.244	-0.053***	-49.55
	2017	0.191	0.244	-0.053***	-49.55
N		320,887	281,765		

Notes: Mean probability of different land cover classes based on Dynamic World annual mean composites from February imagery for a given year and upscaled to 30m resolution. Analysis uses data from Cox Bazar district. Treatment group is 0-5 km from a camp boundary, and control group is > 20 km from nearest camp. Final groupings based on propensity score matching. Stars denote significance levels: * $p < 0.05$, ** $p < 0.01$, *** $p < 0.001$.

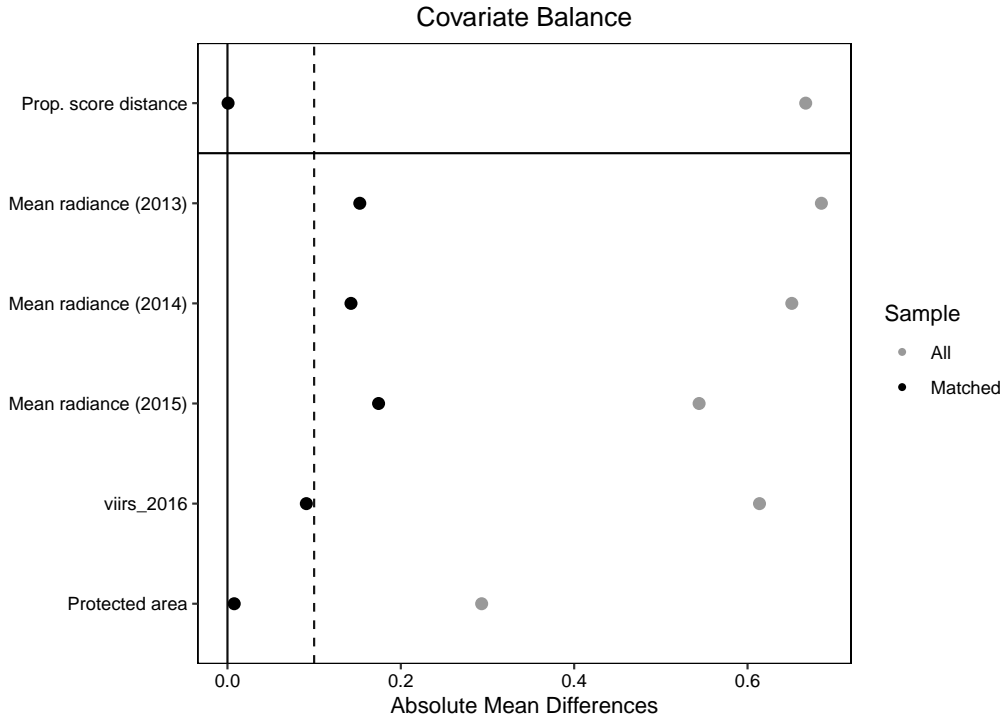
Figure A17: Control group matching cluster grid locations, Banderban district omitted



Notes: Analysis uses data from Cox Bazar district. Treatment group is 0-5 km from a camp boundary, and control group is > 20 km from nearest camp. Final groupings based on propensity score matching. Grids represent the 1km grids used for matching and for clustering standard errors.

B.7 Nighttime radiance

Figure A18: Covariate balancing table from propensity score matching, Nighttime radiance



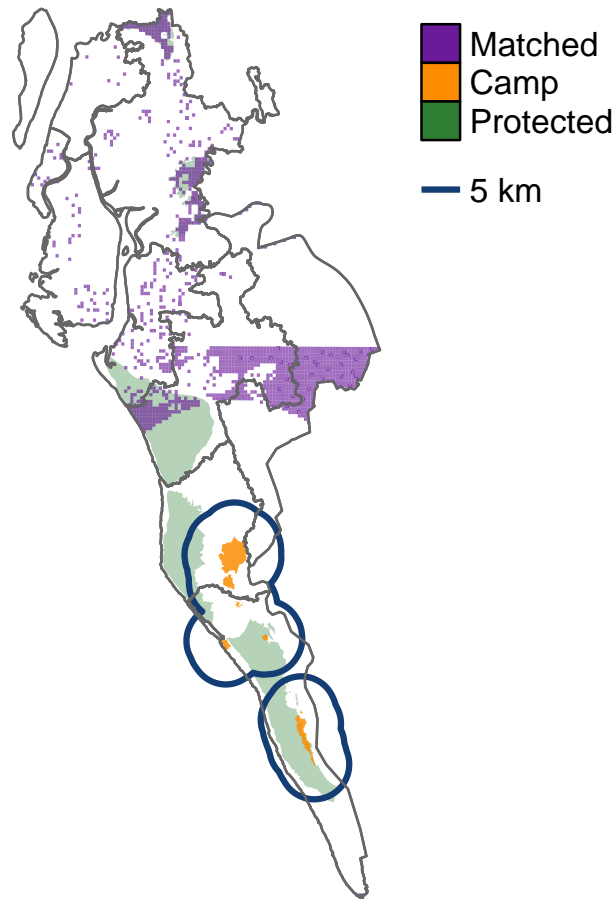
Notes: Mean nighttime radiance based on VIIRS Annual Composites V2.1. Analysis uses data from Cox Bazar district and Nakihongchari subdistrict. Treatment group is 0-5 km from a camp boundary, and control group is > 20 km from nearest camp. Absolute standardized mean differences based on nearest neighbor ($K = 1$) propensity score matching.

Table A8: Balance tests for pre-treatment years, Nighttime radiance

Variable	Year	Control	Treated	Difference	t-stat
Mean radiance	2013	0.075	0.054	0.021**	2.98
	2014	0.069	0.050	0.019**	2.76
	2015	0.097	0.071	0.027***	3.31
	2016	0.062	0.049	0.013	1.89
Protected	2013	0.244	0.236	0.008	0.46
N		1,284	1,284		

Notes: Mean nighttime radiance based on VIIRS Annual Composites V2.1. Analysis uses data from Cox Bazar district and Nakihongchari subdistrict. Treatment group is 0-5 km from a camp boundary, and control group is > 20 km from nearest camp. Final groupings based on propensity score matching. Stars denote significance levels: * $p < 0.05$, ** $p < 0.01$, *** $p < 0.001$.

Figure A19: Control group matching cluster grid locations, Banderban district omitted



Notes: Analysis uses data from Cox Bazar district and Nakihongchari subdistrict. Treatment group is 0-5 km from a camp boundary, and control group is > 20 km from nearest camp. Final groupings based on propensity score matching. Grids reflect the 500m resolution of the VIIRS data.

C Full event study results

C.1 Primary specification

Table A9: Event study coefficient estimates, Primary specification

Year	Outcome Variables			
	(1) Forest	(2) Vegetation	(3) Settlement	(4) Agriculture
2016	-0.003 (0.003)	0.000 (0.002)	0.001 (0.002)	-0.000 (0.002)
2018	-0.037*** (0.004)	0.009*** (0.002)	0.019*** (0.002)	0.005*** (0.002)
2019	-0.046*** (0.004)	0.010*** (0.002)	0.027*** (0.003)	0.004* (0.002)
2020	-0.026*** (0.003)	0.003 (0.002)	0.019*** (0.002)	0.008** (0.003)
2021	-0.029*** (0.004)	-0.001 (0.002)	0.037*** (0.003)	0.002 (0.002)
2022	-0.033*** (0.004)	0.000 (0.002)	0.037*** (0.004)	0.004* (0.002)
2023	-0.017*** (0.004)	-0.002 (0.003)	0.034*** (0.004)	-0.012*** (0.002)
N	5,222,192	5,222,192	5,222,192	5,222,192

Notes: Estimates of Equation 1, with 2017 as the reference year and 2016 coefficient representing the pre-treatment trend. Observations are 30m grid-cells in Cox Bazar district or Nakihongchari subdistrict. Outcome variable is the probability of a given land cover class on the grid cell and is derived using mean composite from Dynamic World February layers for each year. Treatment areas are 0-5 km from nearest camp boundary and are based on the Euclidean distance function. Areas > 5 km and ≤ 20 km from nearest camp boundary are omitted. Analysis uses propensity score matching to match 1km treatment and control gridcells based on pre-treatment and time-invariant observations. 30m observations within the matched 1km gridcells are used in the event study estimation. Standard errors clustered by 1km cluster grid. * $p < 0.10$, ** $p < 0.05$, *** $p < 0.01$.

C.2 Protected areas only

Table A10: Event study coefficient estimates, Protected areas only

Year	Outcome Variables			
	(1) Forest	(2) Vegetation	(3) Settlement	(4) Agriculture
2016	-0.003 (0.008)	0.002 (0.006)	0.007* (0.004)	-0.006 (0.005)
2018	-0.015*** (0.005)	0.011*** (0.003)	-0.002 (0.003)	0.005** (0.002)
2019	-0.032*** (0.007)	0.019*** (0.004)	-0.003 (0.005)	0.015*** (0.003)
2020	-0.013* (0.007)	0.012** (0.005)	0.002 (0.003)	-0.002 (0.003)
2021	-0.006 (0.009)	0.001 (0.006)	0.004 (0.005)	0.006* (0.003)
2022	-0.017* (0.010)	0.020*** (0.006)	-0.009 (0.006)	0.005 (0.004)
2023	0.001 (0.011)	0.015** (0.007)	-0.006 (0.006)	-0.013*** (0.005)
N	661,808	661,808	661,808	661,808

Notes: Estimates of Equation 1, with 2017 as the reference year and 2016 coefficient representing the pre-treatment trend. Observations are 30m grid-cells in Cox Bazar district or Nakihongchari subdistrict that fall in a protected area. Outcome variable is the probability of a given land cover class on the grid cell and is derived using mean composite from Dynamic World February layers for each year. Treatment areas are 0-5 km from nearest camp boundary and are based on the Euclidean distance function. Areas > 5 km and ≤ 20 km from nearest camp boundary are omitted. Analysis uses propensity score matching to match 1km treatment and control gridcells based on pre-treatment and time-invariant observations. 30m observations within the matched 1km gridcells are used in the event study estimation. Standard errors clustered by 1km cluster grid. * $p < 0.10$, ** $p < 0.05$, *** $p < 0.01$.

C.3 Kutapalong Expansion Site vicinity

Table A11: Event-study coefficient estimates, Kutapalong Expansion Site vicinity as treatment area

Year	Outcome Variables			
	(1) Forest	(2) Vegetation	(3) Settlement	(4) Agriculture
2016	0.001 (0.004)	-0.002 (0.002)	-0.004 (0.003)	0.004 (0.002)
2018	-0.046*** (0.005)	0.011*** (0.004)	0.019*** (0.003)	0.014*** (0.002)
2019	-0.058*** (0.007)	0.009*** (0.003)	0.030*** (0.004)	0.008** (0.003)
2020	-0.037*** (0.005)	-0.000 (0.003)	0.020*** (0.002)	0.019*** (0.003)
2021	-0.034*** (0.005)	-0.008*** (0.003)	0.040*** (0.004)	0.005* (0.003)
2022	-0.039*** (0.005)	-0.011*** (0.004)	0.048*** (0.006)	0.006** (0.003)
2023	-0.021*** (0.005)	-0.016*** (0.004)	0.046*** (0.006)	0.000 (0.003)
N	3,033,936	3,033,936	3,033,936	3,033,936

Notes: Estimates of Equation 1, with 2017 as the reference year and 2016 coefficient representing the pre-treatment trend. Observations are 30m grid-cells in Cox Bazar district or Nakihongchari subdistrict. Outcome variable is the probability of a given land cover class on the grid cell and is derived using mean composite from Dynamic World February layers for each year. Treatment areas are 0-5 km from nearest border of the Kutapalong Expansion Site based on the Euclidean distance function. Areas > 5 km and ≤ 20 km from nearest camp boundary are omitted, and all areas 5km south of the bottom extent of the Kutapalong Expansion Site area or further are omitted. Analysis uses propensity score matching to match 1km treatment and control gridcells based on pre-treatment and time-invariant observations. 30m observations within the matched 1km gridcells are used in the event study estimation. Standard errors clustered by 1km cluster grid. * p<0.10, ** p<0.05, *** p<0.01.

C.4 0-10 km treatment area

Table A12: Event-study coefficient estimates, 0-10 km treatment area

Year	Outcome Variables			
	(1) Forest	(2) Vegetation	(3) Settlement	(4) Agriculture
2016	-0.003 (0.003)	-0.002 (0.002)	0.000 (0.002)	0.004** (0.002)
2018	-0.030*** (0.003)	0.003* (0.002)	0.019*** (0.002)	0.005*** (0.002)
2019	-0.036*** (0.003)	0.002 (0.002)	0.027*** (0.003)	0.004** (0.002)
2020	-0.020*** (0.003)	-0.002 (0.002)	0.020*** (0.002)	0.006** (0.002)
2021	-0.023*** (0.003)	-0.007*** (0.002)	0.037*** (0.003)	-0.000 (0.002)
2022	-0.028*** (0.003)	-0.005** (0.002)	0.033*** (0.003)	0.004* (0.002)
2023	-0.014*** (0.003)	-0.006*** (0.002)	0.035*** (0.004)	-0.011*** (0.002)
N	7,740,408	7,740,408	7,740,408	7,740,408

Notes: Estimates of Equation 1, with 2017 as the reference year and 2016 coefficient representing the pre-treatment trend. Observations are 30m grid-cells in Cox Bazar district or Nakihongchari subdistrict. Outcome variable is the probability of a given land cover class on the grid cell and is derived using mean composite from Dynamic World February layers for each year. Treatment areas are 0-10 km from nearest camp boundary and are based on the Euclidean distance function. Areas > 10 km and ≤ 20 km from nearest camp boundary are omitted. Analysis uses propensity score matching to match 1km treatment and control gridcells based on pre-treatment and time-invariant observations. 30m observations within the matched 1km gridcells are used in the event study estimation. Standard errors clustered by 1km cluster grid. * $p < 0.10$, ** $p < 0.05$, *** $p < 0.01$.

C.5 Chittagong comparison sample

Table A13: Event-study coefficient estimates, Chittagong comparison area)

Year	Outcome Variables			
	(1) Forest	(2) Vegetation	(3) Settlement	(4) Agriculture
2016	0.003 (0.005)	-0.001 (0.004)	0.003 (0.003)	0.004 (0.003)
2018	-0.029*** (0.008)	0.022*** (0.005)	0.005 (0.003)	-0.009*** (0.003)
2019	-0.050*** (0.009)	0.012** (0.005)	0.006 (0.004)	0.010** (0.004)
2020	-0.040*** (0.007)	0.004 (0.004)	0.012*** (0.002)	0.021*** (0.004)
2021	-0.017*** (0.006)	-0.002 (0.004)	0.025*** (0.004)	0.008** (0.003)
2022	-0.024*** (0.007)	0.001 (0.004)	0.019*** (0.006)	0.005 (0.004)
2023	-0.004 (0.007)	-0.001 (0.005)	0.032*** (0.006)	-0.004 (0.003)
N	2,023,416	2,023,416	2,023,416	2,023,416

Notes: Estimates of Equation 1, with 2017 as the reference year and 2016 coefficient representing the pre-treatment trend. Observations are 30m grid-cells in Cox Bazar district or Naikhongchari subdistrict that are 0-5 km from nearest camp boundary or are sourced from the Chittagong district. Outcome variable is the probability of a given land cover class on the grid cell and is derived using mean composite from Dynamic World February layers for each year. Treatment areas are 0-5 km from nearest camp boundary and are based on the Euclidean distance function. All other areas of Cox Bazar and Naikhongchari are omitted. Analysis uses propensity score matching to match 1km treatment and control gridcells based on pre-treatment and time-invariant observations. 30m observations within the matched 1km gridcells are used in the event study estimation. Standard errors clustered by 1km cluster grid. * p<0.10, ** p<0.05, *** p<0.01.

C.6 Omitting Banderban

Table A14: Event-study coefficient estimates, Banderban district omitted)

Year	Outcome Variables			
	(1) Forest	(2) Vegetation	(3) Settlement	(4) Agriculture
2016	-0.006* (0.003)	0.004* (0.002)	0.000 (0.002)	-0.001 (0.003)
2018	-0.034*** (0.004)	0.008*** (0.002)	0.018*** (0.003)	0.005** (0.002)
2019	-0.043*** (0.005)	0.009*** (0.003)	0.026*** (0.003)	0.005* (0.003)
2020	-0.024*** (0.004)	0.004* (0.002)	0.019*** (0.002)	0.009*** (0.003)
2021	-0.027*** (0.004)	-0.000 (0.002)	0.035*** (0.003)	0.003 (0.002)
2022	-0.032*** (0.004)	0.001 (0.003)	0.035*** (0.004)	0.005* (0.002)
2023	-0.018*** (0.004)	0.002 (0.003)	0.030*** (0.004)	-0.012*** (0.002)
N	4,821,216	4,821,216	4,821,216	4,821,216

Notes: Estimates of Equation 1, with 2017 as the reference year and 2016 coefficient representing the pre-treatment trend. Observations are 30m grid-cells in Cox Bazar district. Outcome variable is the probability of a given land cover class on the grid cell and is derived using mean composite from Dynamic World February layers for each year. Treatment areas are 0-5 km from nearest camp boundary and are based on the Euclidean distance function. Areas > 5 km and ≤ 20 km from nearest camp boundary are omitted. Analysis uses propensity score matching to match 1km treatment and control gridcells based on pre-treatment and time-invariant observations. 30m observations within the matched 1km gridcells are used in the event study estimation. Standard errors clustered by 1km cluster grid. * p<0.10, ** p<0.05, *** p<0.01.

C.7 Nighttime radiance

Table A15: Event-study coefficient estimates, nighttime radiance

Year	Outcome Variables
	(1) Radiance
2013	-0.008 (0.005)
2014	-0.006 (0.006)
2015	-0.013* (0.007)
2017	-0.001 (0.017)
2018	0.075** (0.033)
2019	0.123*** (0.046)
2020	0.175*** (0.052)
2021	0.200*** (0.062)
N	23,112

Notes: Estimates of Equation 1, with 2016 as the reference year and 2013–2015 representing pre-treatment years. Observations are 500 m grid-cells in Cox’s Bazar district or Naikhongchari subdistrict. The outcome is mean nighttime lights radiance (VIIRS Annual Composite V2.1). Treatment areas are 0–5 km from the nearest camp boundary. Areas > 5 km and ≤ 20 km are omitted. Propensity score matching uses pre-treatment and time-invariant covariates. Standard errors are clustered by 2 km cluster grid. * p<0.10, ** p<0.05, *** p<0.01.